Emeis, K.-C., Robertson, A.H.F., Richter, C., et al., 1996
Proceedings of the Ocean Drilling Program, Initial Reports, Vol. 160

12. SITE 971[1]

Shipboard Scientific Party[2]

HOLE 971A

Date occupied: 20 April 1995

Date departed: 21 April 1995

Time on hole: 16 hr, 30 min

Position: 33°42.190′N, 24°42.814′E

Bottom felt (drill-pipe measurement from rig floor, m): 2037.5

Distance between rig floor and sea level (m): 11.4

Water depth (drill-pipe measurement from sea level, m): 2026.1

Total depth (from rig floor, m): 2143.4

Penetration (m): 105.9

Number of cores (including cores having no recovery): 12

Total length of cored section (m): 105.9

Total core recovered (m): 58.8

Core recovery (%): 55.5

Oldest sediment cored:
Depth (mbsf): 105.90
Nature: nannofossil ooze
Earliest age: late Pliocene

HOLE 971B

Date occupied: 21 April 1995

Date departed: 23 April 1995

Time on hole: 2 days, 09 hr

Position: 33°42.817′N, 24°42.108′E

Bottom felt (drill-pipe measurement from rig floor, m): 2152.3

Distance between rig floor and sea level (m): 11.4

Water depth (drill-pipe measurement from sea level, m): 2140.9

Total depth (from rig floor, m): 2355.8

Penetration (m): 203.5

Number of cores (including cores having no recovery): 22

Total length of cored section (m): 203.5

Total core recovered (m): 64.2

Core recovery (%): 31.5

Oldest sediment cored:
Depth (mbsf): 203.50
Nature: debris-flow deposits
Earliest age: Pleistocene

HOLE 971C

Date occupied: 23 April 1995

Date departed: 23 April 1995

Time on hole: 02 hr, 15 min

Position: 33°42.818′N, 24°42.108′E

Bottom felt (drill-pipe measurement from rig floor, m): 2152.3

Distance between rig floor and sea level (m): 11.4

Water depth (drill-pipe measurement from sea level, m): 2140.9

Total depth (from rig floor, m): 2169.0

Penetration (m): 16.7

Number of cores (including cores having no recovery): 2

Total length of cored section (m): 16.7

Total core recovered (m): 17.3

Core recovery (%): 103.3

Oldest sediment cored:
Depth (mbsf): 16.70
Nature: nannofossil clay
Earliest age: late Pleistocene
Latest age: middle Pleistocene

HOLE 971D

Date occupied: 23 April 1995

Date departed: 24 April 1995

Time on hole: 09 hr

Position: 33°43.437′N, 24°41.276′E

Bottom felt (drill-pipe measurement from rig floor, m): 1944.5

Distance between rig floor and sea level (m): 11.4

Water depth (drill-pipe measurement from sea level, m): 1933.1

Total depth (from rig floor, m): 1990.5

Penetration (m): 46.0

Number of cores (including cores having no recovery): 5

Total length of cored section (m): 46.0

Total core recovered (m): 47.5

Core recovery (%): 103.3

Oldest sediment cored:
Depth (mbsf): 46.00
Nature: silty clay
Earliest age: Pleistocene
Measured velocity (km/s): 2.0

HOLE 971E

Date occupied: 24 April 1995

[1] Emeis, K.-C., Robertson, A.H.F., Richter, C., et al., 1996. *Proc. ODP, Init. Repts.,* 160: College Station, TX (Ocean Drilling Program).

[2] Shipboard Scientific Party is given in the list preceding the Table of Contents.

Date departed: 25 April 1995

Time on hole: 10 hr

Position: 33°43.621′N, 24°40.839′E

Bottom felt (drill-pipe measurement from rig floor, m): 1955.0

Distance between rig floor and sea level (m): 11.4

Water depth (drill-pipe measurement from sea level, m): 1943.6

Total depth (from rig floor, m): 1983.5

Penetration (m): 28.5

Number of cores (including cores having no recovery): 3

Total length of cored section (m): 28.5

Total core recovered (m): 29.5

Core recovery (%): 103.6

Oldest sediment cored:
Depth (mbsf): 28.50
Nature: silty clay
Earliest age: Pleistocene

Principal results: A transect of four holes was drilled from the flank to the crest of the Napoli mud structure to shed light on its age and origin. An additional hole was drilled in an area of the crest where the active venting of gas was known to exist. The outer flank sediments (Hole 971A), of Pleistocene to middle Pliocene age, are underlain by clast-rich, matrix-supported sediments (breccia/conglomerate), interpreted as debris flows. The clasts are mainly calcareous and range up to several centimeters in size. Microfossils of Pleistocene, middle Miocene, Oligocene, and Eocene age are present in the matrix of the debris flows. Clasts in the mud debris flows are of Miocene age, but also contain reworked microfossils of Oligocene, Eocene, and Cretaceous age. Sediments in a seismically imaged moat structure (Hole 971B) are dominated by mud debris flows, which contain relatively small numbers of clasts, mainly of clay. Formation MicroScanner logging data, although of poor quality, reveal distinct cyclicity within the debris flows. An additional hole (Hole 971C) was drilled in the moat to recover a thick sapropel in which diatoms and some radiolarians are preserved, including species characteristic of upwelling areas and mat-forming varieties. The diatoms were most likely preserved as a result of high sedimentation rates and a favorable diagenetic environment. By contrast, sediment at the crestal sites (Holes 971D and 971E) is dominated by silty and sandy clays, which commonly exhibit a mousselike (i.e., gaseous) texture. Fragments of crystalline halite and rare halite-cemented clasts were also noted.

Hydrocarbon gas was found actively venting from the Napoli mud volcano during the site surveys, and pure methane was encountered in gas bubbles within sediments on the crest of the Napoli mud volcano. However, gas hydrates were not observed, in contrast to the Milano mud volcano. Higher hydrocarbons are present, but they could not all be identified on the ship. The pore waters are saturated with respect to halite in each of the holes drilled. The potassium-rich nature of some of the brines suggests that more than one source of evaporite-derived fluid may be present. Very high alkalinity throughout probably reflects microbial consumption of methane. A local downward decrease in sulfate suggests high bacterial sulfate-reduction rates and an organic-matter-rich substrate.

The Napoli mud structure is interpreted, based on micropaleontological evidence, as a mud volcano that became active between 1.5 and 1.25 Ma and has remained episodically active to the present time.

BACKGROUND AND OBJECTIVES

Site 971 constituted the second of the two transects of holes across mud mound structures on the Mediterranean Ridge (Fig. 1). The objective of this site was to core the impressive Napoli Dome (>2 km across and 100 m high; see "Tectonic Introduction" chapter, this volume). The Napoli structure is known to be currently active, because cores have been found to be gas rich, and an underwater video made by *Gelendzhik* in 1993 revealed evidence of discrete vents emitting fluids and surrounded by an oasis of life, including bacterial mats and large-shelled bivalves. Seismic evidence does not reveal any internal structure, and on narrow-beam side-scan sonar the structure is relatively transparent, in contrast with the reflective character shown by many of the other mud structures (Limonov et al., 1994). The fact that this structure is active (i.e., venting of gases and fluids) provides an opportunity to make useful comparisons with the Milano structure at Site 970, which was believed inactive.

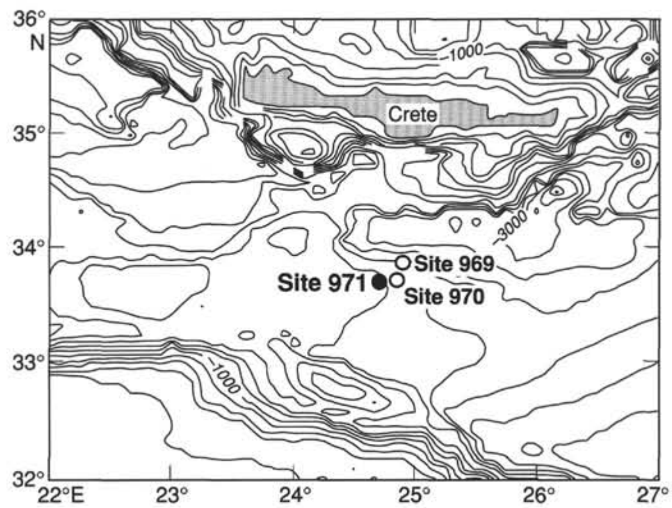

Figure 1. Outline map showing the location of Site 971.

The strategy at Site 971 was to drill a transect of three holes from the flank to the crest of the dome and an additional hole in an active vent area. Hole 971A was located on a small raised area beyond a rim depression, where we hoped to drill through materials (flows or sills) related to construction of the dome into background Pliocene-Quaternary sediments beneath. This would date the time of initiation of the mud structure and reveal information on its processes of construction. The second hole (Hole 971B) was located in a moatlike depression, with the aim of showing if the structure is composed of mud flows or sills. The third transect hole was located on the crest of the structure (restricted to 50 mbsf by safety considerations), where we hoped to determine the nature of the sediment and of any active geochemical processes. The additional hole (Hole 971D, also restricted to 50 mbsf) was located on the upper flanks, not far from the crest, close to where underwater video had revealed evidence of active fluid venting.

In summary, the main objectives of drilling the Napoli mud dome were (1) to determine its cross-sectional anatomy and processes of construction, including possible intrusion of mud sills and extrusion of mud flows; (2) to infer the origin and deep structure of the mud dome by dating of clasts known to be present within muds based on coring; (3) to determine the physical and chemical properties of the mud structure; (4) to document active processes, notably fluid flow, within a young, active mud structure by means of pore-fluid chemistry, temperature measurements, and logging; and (5) to make comparisons with the apparently less-active Milano mud structure drilled at Site 970 and to try to test existing models of the evolution of the mud structures, in which both the Napoli and Milano structures could represent different stages. This could, in turn, lead to a new interpretation of the origin of these mud volcanoes.

GEOLOGICAL SETTING

The second of the structures to be drilled, at Site 971, is the Napoli mud dome. The Napoli mud dome is well known, following detailed seismic reflection, bathymetric, and coring studies by a number of recent expeditions (Fig. 2). Additional information was provided by the Site 971 site survey (see "Site Geophysics" section, this chapter).

The Napoli mud dome differs from some other structures in the Olimpi mud field as it is relatively flat topped rather than conical (Camerlenghi et al., 1995). The flanks are marked by a series of steplike features. Similar structures are seen seaward of the Barbados Ridge (Henry et al., 1990; Brown and Westbrook, 1988). Seismic studies reveal virtually no structure in, or around, the Napoli Dome, in contrast to many of the other mud edifices, which appear to interfinger with the background Pliocene-Quaternary sediments.

Important information on the Napoli mud structure was provided recently by both wide- and narrow-beam side-scan sonar records obtained by *Gelendzhik* in 1993 (Limonov et al., 1994). On the wide-beam OKEAN records, many of the mud domes show up as dark features, owing to high reflectivity. On the other hand, the Napoli Dome is a nearly transparent, low-reflectivity feature. The high-reflectivity patches were inferred to represent seafloor developments of mud breccia. Coring confirmed this. In some cases, such features were partly obscured by what was interpreted as a thin veneer of background sediment. The OKEAN mapping also indicated that the Olimpi Field appears to be partly surrounded by a series of broadly concentric folds. These features were tentatively interpreted as the result of outward expansion and compression from a large domelike structure rising within the Olimpi Field. This "bulging" may relate to large-scale uprise of fluidized mud that has become overpressured in the backthrust zone, where the Mediterranean Ridge is thrust over an inferred backstop to the north. Fluid pressures could have built up beneath a seal of Messinian evaporite that was then broken by thrusting, which allowed the fluidized material to escape. It is also possible that strike-slip faulting, related to the formation of the Pliny Trench, might have helped to break a seal. Interestingly, there is a similar concentration of mud domes adjacent to the Strabo Trench farther east along the ridge crest, in an area that is again influenced by strike-slip faulting (Limonov et al., 1994).

Greater detail of the Napoli Dome was provided by high-resolution narrow-beam MAK-1 sonar records (Fig. 3). These reveal semicircular lineation patterns that are interpreted as debris flows composed of mud breccia. In the vicinity, the Toronto Dome is most convincingly imaged as a mud volcano (Fig. 4). Circular patches within the inferred mud debris flows could represent flank eruptions. In addition, a number of visible terraces may record the effects of mud debris flowing over an irregularly sloping topography. Small dark patches are concentrated in some areas of the upper flanks and could represent fluid vent structures.

A number of cores taken on the Napoli Dome from the *Bannock* cruise are shown in Figure 5. Additional wide-diameter cores were taken during the 1993 *Gelendzhik* cruise (Limonov et al., 1994; Fig. 6). Three cores comprise "mud breccia" overlain by a veneer of pelagic sediments (Holocene oozes). The mud breccia has a mousselike (i.e., gaseous) texture and contains abundant millimeter-sized voids, inferred to have resulted from gas expansion. These cores have an odor of hydrogen sulfide. The mud mousse becomes finer grained upward and passes transitionally into pelagic marl. The boundary between the mud breccia and the overlying Holocene ooze is marked by an oxidized interval up to 10 cm thick. A number of different types of mud breccia were recorded (Staffini et al., 1993). Smear slides from the mud matrix reveal high contents of clay, dolomite, nannofossils, quartz, and sporadically abundant pyrite. Nineteen samples were analyzed for foraminifers. The ages range from late Eocene to Pliocene, with well-preserved Quaternary species.

Underwater video profiles were made across both the Napoli and Moscow mud volcanoes in the Olimpi area. These represent a view of only 1 or 2 m. Interpretation is complicated by the effect of sediment resuspension caused by the video apparatus glancing against the seafloor. The first video crossed the Napoli Dome from the depression along the southeast side, up the slope, and across the volcano axial zones in a northwest direction, ending on the opposite slope. The bottom sediments away from the mud volcano are yellowish brown

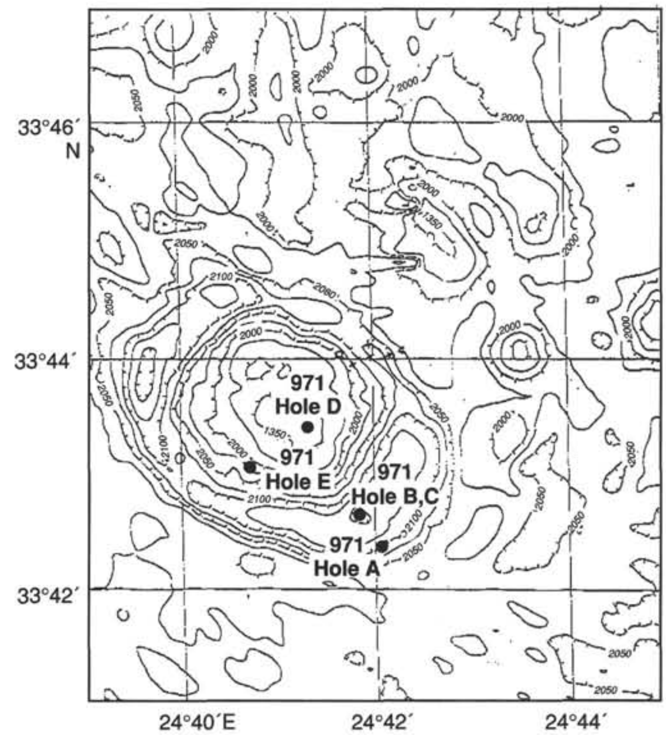

Figure 2. Hydrosweep map of the Napoli mud volcano, produced aboard *Meteor* in July 1993, modified to show the Site 971 holes (courtesy of W. Hieke).

mud, similar to those seen at the tops of the cores taken in the area. On the flanks of the mud volcano are patches and strips of dark gray heterogeneous material that appears to be coarse, possibly even gravelly. The dark patches exhibit sharp boundaries with the lighter background sediments and appear to fill bottom depressions and/or suggest the existence of downslope gravity flows. These features are tentatively interpreted as the result of mud debris flowing down the flanks of the volcano and/or preferentially collecting on the upper part of the upper plateau. In addition, two types of black holes were observed. The first type of hole is small (<10 cm) in diameter and mostly circular. These are commonly partially rimmed with unidentified white matter, which gives a horseshoe-shaped appearance. Some of the holes are aligned in rows that appear to roughly parallel the dip of the slope. The second type of hole is larger (50 cm to 1 m) and more irregularly shaped, again with partial rims of white material. Tracks up to 1 m long and 5–10 cm across are inferred to be the traces of unidentified fauna. Some of the larger holes are associated with a blocky structure that could be organic in origin. Varicolored crusts cover some of the blocky features and could be bacterial mats. In several locations, vents were observed, from which the emission of fluids and muds was seen. Large numbers of shells are also present near these vents.

In summary, in contrast to the Milano mud dome drilled at Site 970, the Napoli Dome is interpreted as a still-active structure that can contribute much to understanding the processes of mud volcanism or mud diapirism.

OPERATIONS

Transit to Site 971

The ship was moved in dynamic-positioning mode 3.7 nmi west of Site 970 in 3.5 hr, and a Datasonics 354M beacon (S/N 779, 15.0 kHz) was dropped at 1401 hr on 20 April.

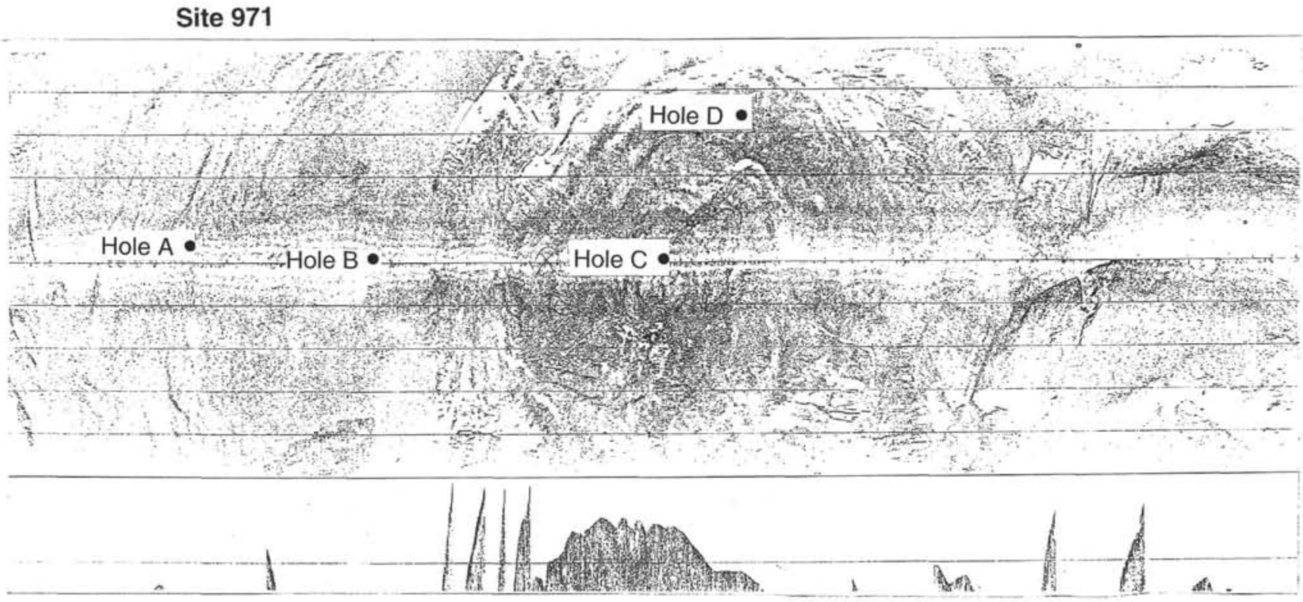

Figure 3. MAK-1 high-resolution side-scan sonar image of the summit and flanks of the Napoli mud dome. The approximate location of the sites drilled is marked. From data collected by *Gelendzhik*.

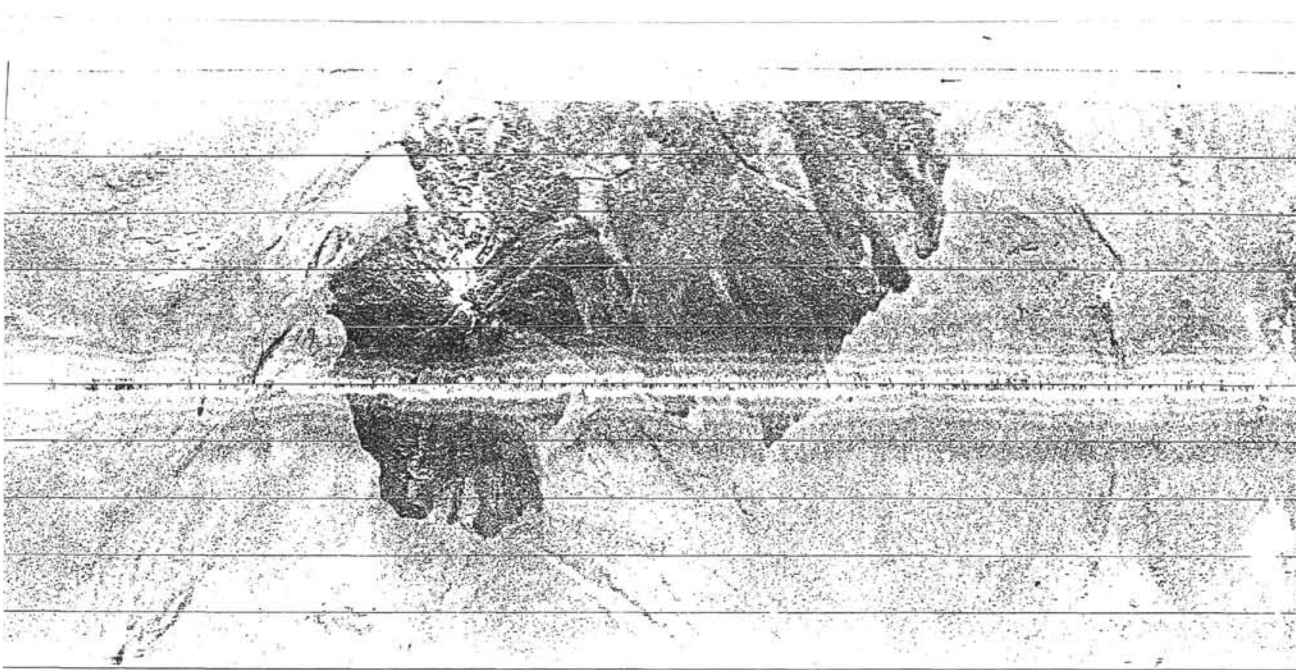

Figure 4. MAK-1 high-resolution side-scan sonar image of the summit and flanks of the Toronto mud dome (1993 MAK-1 Line 18; see Limonov et al., 1994) clearly images the mud volcano-like structure, with radiating debris flows.

Hole 971A

Hole 971A (proposed Sites MV-1/1 and MV-1/2) was spudded at 1600 hr on 20 April on the distal flank of the Napoli mud volcano. The estimated seafloor depth was at 2026.1 m by drill-pipe measurement (DPM). APC Cores 160-971A-1H through 4H were taken from 0 to 28.5 mbsf (Table 1), with 28.5 m cored and 28.94 m recovered (101.5% recovery). The last two cores were partial strokes in hard clay with pebbles and gravel, and Core 160-971A-4H required 25 min to drill off in hard siltstone. XCB Cores 160-971A-5X through 12X were taken from 28.5 to 105.9 mbsf, with 77.4 m cored and 29.81 m recovered (38.5% recovery). A short hard-formation shoe and 8- and 9-finger core catchers were used. Overall recovery was 55.5%. The bit cleared the seafloor at 0635 hr on 21 April and the beacon was recovered.

Hole 971B

The ship was moved 0.87 nmi northwest to the flank moat of the Napoli mud volcano, and a Datasonics 354M beacon (S/N 1243, 14.0

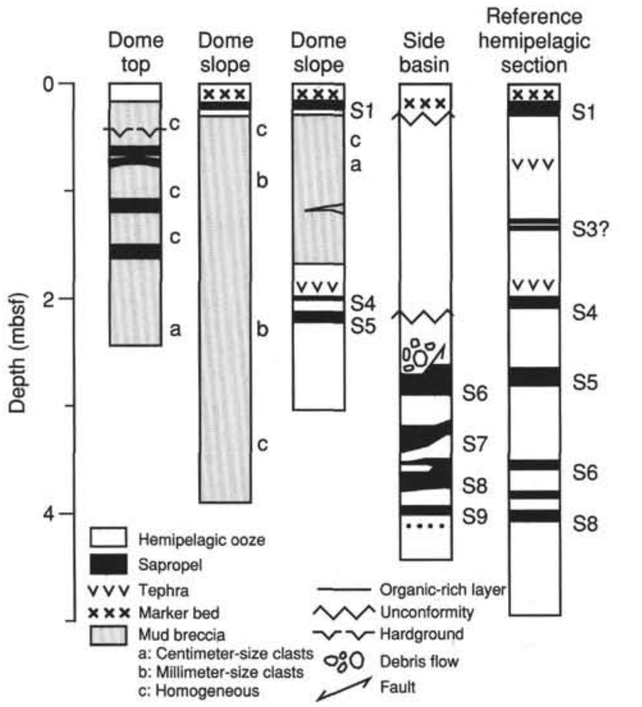

Figure 5. Simplified core logs of the cores recovered from the Napoli mud dome during the *Bannock* cruise (after Camerlenghi et al., 1992).

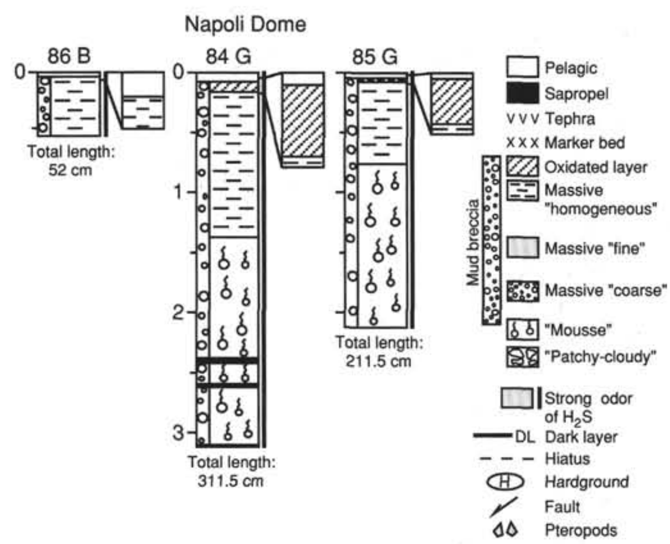

Figure 6. Cores taken from the Napoli Dome by *Gelendzhik* in 1993 (Limonov et al., 1994).

kHz) was dropped at 0802 hr on 21 April. Special H_2S and hydrocarbon guidelines were approved by the Pollution Prevention and Safety Panel for this site, which has active natural venting. Hole 971B was spudded at 1015 hr on 21 April. The seafloor depth was 2140.9 m DPM. APC Cores 160-971B-1H through 4H were taken from 0 to 30.7 mbsf (Table 1), with 30.7 m cored and 31.37 m recovered (102.2% recovery). XCB Cores 160-971B-5X through 22X were taken from 30.7 to 203.5 mbsf, with 172.8 m cored and 33.04 m recovered (19.1% recovery). A short hard-formation shoe and 8- and 9-finger core catchers were used. Six of the 18 XCB cores jammed in the shoe. Overall recovery was 31.5%.

Table 1. Coring summary for Site 971.

Core	Date (April 1995)	Time (UTC)	Depth (mbsf)	Length cored (m)	Length recovered (m)	Recovery (%)
160-971A-						
1H	20	1415	0.0–7.0	7.0	7.03	100.0
2H	20	1455	7.0–16.5	9.5	10.00	105.2
3H	20	1530	16.5–22.5	6.0	5.83	97.1
4H	20	1605	22.5–28.5	6.0	6.08	101.0
5X	20	1810	28.5–38.2	9.7	0.43	4.4
6X	20	1955	38.2–47.9	9.7	1.10	11.3
7X	20	2130	47.9–57.6	9.7	0.79	8.1
8X	20	2310	57.6–67.3	9.7	0.83	8.6
9X	21	0020	67.3–77.0	9.7	0.43	4.4
10X	21	0130	77.0–86.7	9.7	8.54	88.0
11X	21	0235	86.7–96.3	9.6	8.21	85.5
12X	21	0345	96.3–105.9	9.6	9.48	98.7
Coring totals:				105.9	58.8	55.5
160-971B-						
1H	21	0830	0.0–2.2	2.2	2.19	99.5
2H	21	0905	2.2–11.7	9.5	9.81	103.0
3H	21	0935	11.7–21.2	9.5	9.83	103.0
4H	21	1035	21.2–30.7	9.5	9.54	100.0
5X	21	1415	30.7–39.7	9.0	0.00	0.0
6X	21	1555	39.7–49.3	9.6	0.60	6.3
7X	21	1750	49.3–58.9	9.6	1.38	14.4
8X	21	2000	58.9–68.6	9.7	1.11	11.4
9X	21	2215	68.6–78.2	9.6	1.46	15.2
10X	21	2350	78.2–87.9	9.7	0.00	0.0
11X	22	0150	87.9–97.5	9.6	0.00	0.0
12X	22	0425	97.5–107.1	9.6	1.78	18.5
13X	22	0555	107.1–116.7	9.6	2.51	26.1
14X	22	0705	116.7–126.3	9.6	2.86	29.8
15X	22	0815	126.3–136.0	9.7	1.48	15.2
16X	22	1040	136.0–145.6	9.6	4.47	46.5
17X	22	1235	145.6–155.2	9.6	3.46	36.0
18X	22	1420	155.2–164.9	9.7	0.13	1.3
19X	22	1610	164.9–174.5	9.6	7.38	76.9
20X	22	1830	174.5–184.1	9.6	3.53	36.8
21X	22	2045	184.1–193.8	9.7	0.00	0.0
22X	22	2320	193.8–203.5	9.7	0.67	6.9
Coring totals:				203.5	64.2	31.5
160-971C-						
1H	23	1450	0.0–7.2	7.2	7.21	100.0
2H	23	1525	7.2–16.7	9.5	10.04	105.7
Coring totals:				16.7	17.3	103.3
160-971D-						
1H	23	2105	0.0–8.0	8.0	8.05	100.0
2H	23	2135	8.0–17.5	9.5	9.16	96.4
3H	23	2215	17.5–27.0	9.5	10.00	105.2
4H	23	2250	27.0–36.5	9.5	10.14	106.7
5H	23	2350	36.5–46.0	9.5	10.15	106.8
Coring totals:				46.0	47.5	103.3
160-971E-						
1H	24	0410	0.0–9.5	9.5	10.20	107.3
2H	24	0450	9.5–19.0	9.5	10.13	106.6
3H	24	0515	19.0–28.5	9.5	9.19	96.7
Coring totals:				28.5	29.5	103.6

Logging Operations at Hole 971B

A short trip was made to condition the hole for logs, with no drag and 20.8 m of light fill on the bottom. The hole was displaced with 160 bbl of seawater with 2% KCl, and the go-devil was dropped. The pipe was pulled back to 84 mbsf for logging. The induction/sonic log was run to 2325 m below rig floor (mbrf) total depth (TD) (30.8-m fill) in 2.92 hr. The density/neutron log was run to 2288 mbrf TD (67.8-m fill) in 2.75 hr. The FMS log was run to 2280 mbrf TD (75.8-m fill) in 2.25 hr. Logging was finished at 1500 hr on 23 April. The bit cleared the seafloor at 1533 hr on 23 April.

Hole 971C

A short APC hole was required to recover a rare diatom-rich sapropel section missing in the Hole 971B core overlap from 10.2 to 11.7 mbsf. The ship was moved 10 m to the north, and Hole 971C was spudded at 1635 hr on 23 April in the lower flank moat of the Napoli mud volcano. The estimated seafloor depth was 2140.9 m DPM. APC Cores 160-971B-1H and 2H were taken from 0 to 16.7 mbsf, with 16.7 m cored and 17.25 m recovered (103.3% recovery). The bit cleared the seafloor at 1743 hr on 23 April. The beacon was recovered at 1900 hr.

Hole 971D

The ship was moved in dynamic-positioning mode 0.935 nmi northwest to the crest of the Napoli mud volcano, and a beacon was dropped at 1943 hr on 23 April. The first spud attempt resulted in a full core barrel of very gassy clay. The bit was pulled up 5 m, and Hole 971D was spudded at 2235 hr on 23 April. The seafloor was at 1933.1 m DPM. APC Cores 160-971D-1H through 5H (Table 1) were taken from 0 to 46.0 mbsf, with 46.0 m cored and 47.50 m recovered (103.3% recovery). ADARA heat-flow measurements were taken at Core 160-971D-5H.

Core 160-971D-1H had 100–200 ppm H_2S in the top section. The H_2S concentration degassed rapidly to 10 ppm with a negligible ambient level. In the bottom sections, the core was very gassy and expanded (like a mousse) with a slight petroleum odor and 5–10 ppm H_2S. The liners were drilled and allowed to degas on the core platform until the H_2S was 5 ppm or less. Personnel wore air packs in the laboratory while cutting the liners, and the liners were allowed to degas on the core deck with maximum H_2S ambient levels of 5 ppm. The bit cleared the seafloor at 0240 hr on 24 April.

Hole 971E

The ship was moved in dynamic-positioning mode 0.525 nmi southwest to the crestal vent area of Napoli mud volcano, and a Datasonics 354M beacon (S/N 1243, 14.0 kHz) was dropped at 0347 hr on 24 April. Hole 971E was spudded at 0610 hr on 24 April. The seafloor was at 1943.6 m DPM. APC Cores 160-971E-1H through 3H were taken from 1955.0 to 1983.5 m (0–28.5 mbsf), with 28.5 m cored and 29.52 m recovered (103.6% recovery). Core 160-971E-1H was very gassy and had 200 ppm H_2S in the top two sections. On Core 160-971E-3H the core liner burst on the core deck while being drilled to vent gas. There were no injuries, but coring was terminated for crew safety. The bit cleared the seafloor at 0825 on 24 April, and the BHA was secured to end Site 971. The beacon was recovered.

SITE GEOPHYSICS

Site 971 is situated at the Napoli mud dome, the second of the two mud structures selected as ODP drilling targets. There are numerous differences between the Napoli and Milano domes, including the acoustic signature and morphology. Napoli is a dome of low reflectivity in the form of a derby, with a depression surrounding the central dome, but Milano is a sonar-bright dome in the shape of a wide-brimmed mexican hat. The mud forming the surface sediments of the Napoli Dome was found in previous coring (Limonov et al., 1994; Cita et al., 1994) to contain mainly small clasts and gas, which gives the mud a characteristic mousselike texture (see also "Geological Setting" section, this chapter). The lack of large clasts and the presence of distributed gas were considered two of the reasons why the acoustic appearance of the Napoli mud dome is one of low reflectivity in side-scan sonar images (Volgin and Woodside, in press). The Napoli Dome is larger than the Milano Dome.

Two seismic lines were made across Napoli Dome as part of the predrilling site survey (Figs. 7, 8). The east-northeast- to west-southwest-directed line followed a *Bannock* site-survey line, and the northwest to southeast line followed a deep-tow *Gelendzhik* site-survey line. Both seismic profiles show the subsurface structure of the Napoli mud dome to resemble a roughly symmetrical cone, tapering to a width of less than 1 km at a depth of 4.0 s two-way traveltime (TWT) from a seafloor width of greater than 10 km. Few coherent reflectors are visible in the main body of the mud dome above depths of 3.5 s TWT, but the edges of this apparently disorganized mass are defined by the diffractions at the edges of the sedimentary layers that are truncated at the edge of the subsurface structure. A concave-upward reflector is situated at about 3.4 s TWT below the center of the dome, at the same depth as a similar reflector beneath the Milano mud dome. Two strong reflectors were observed beneath the western part of the rim depression at depths of about 3.4 and 3.7 s TWT and dipping to the west.

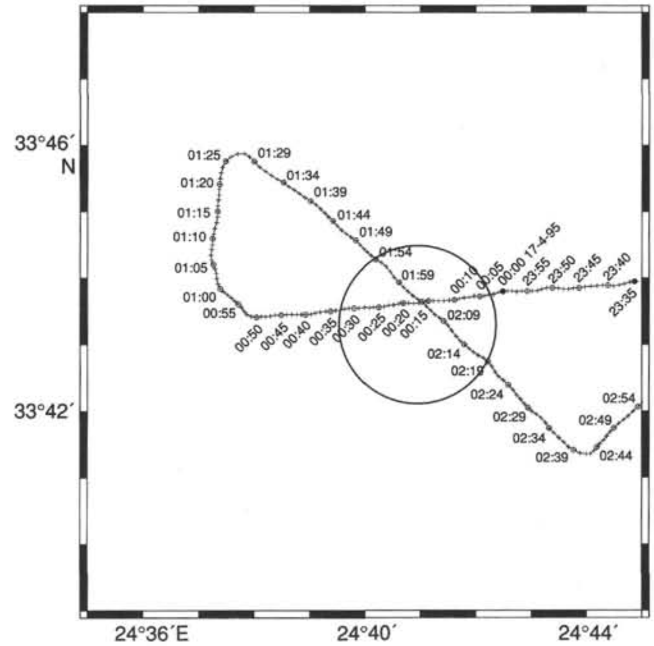

Figure 7. Track chart showing predrilling site-survey lines across the Napoli mud dome at Site 971.

Because sediments cored from the Napoli mud dome contain considerable quantities of gas, often expanding to twice the core diameter as the pressure is released when the cored mud is examined on the deck of the ship (Cita et al., in press), the seismic profiles were examined for evidence of gas concentrations. Beneath the rim bulge to the northwest and the southeast are strong discontinuous reflectors suggestive of "bright spots" resulting from gas; however, there was no indication of phase reversals in the seismic signal that would be expected for such gas accumulations. Likewise, there were no BSRs characteristic of the base of a zone of gas hydrates. However, the seismic system is insufficient to resolve any BSRs that might be present in approximately the upper 100 ms TWT, thus limiting the possible extent of any gas hydrates, if present, to the upper sediments. The seismic evidence at this stage is inconclusive regarding the presence of gas concentrations within the mud dome.

Three of the holes (Holes 971A, 971B, and 971C) were selected on the site-survey line crossing the southern margin of the mud dome. A fourth site (Hole 971D) on the cross line was selected as an optional drilling location (see "Background and Objectives" section, this chapter).

LITHOSTRATIGRAPHY

In the five holes cored at Site 971, two lithostratigraphic units were identified on the basis of visual observation of color, sedimen-

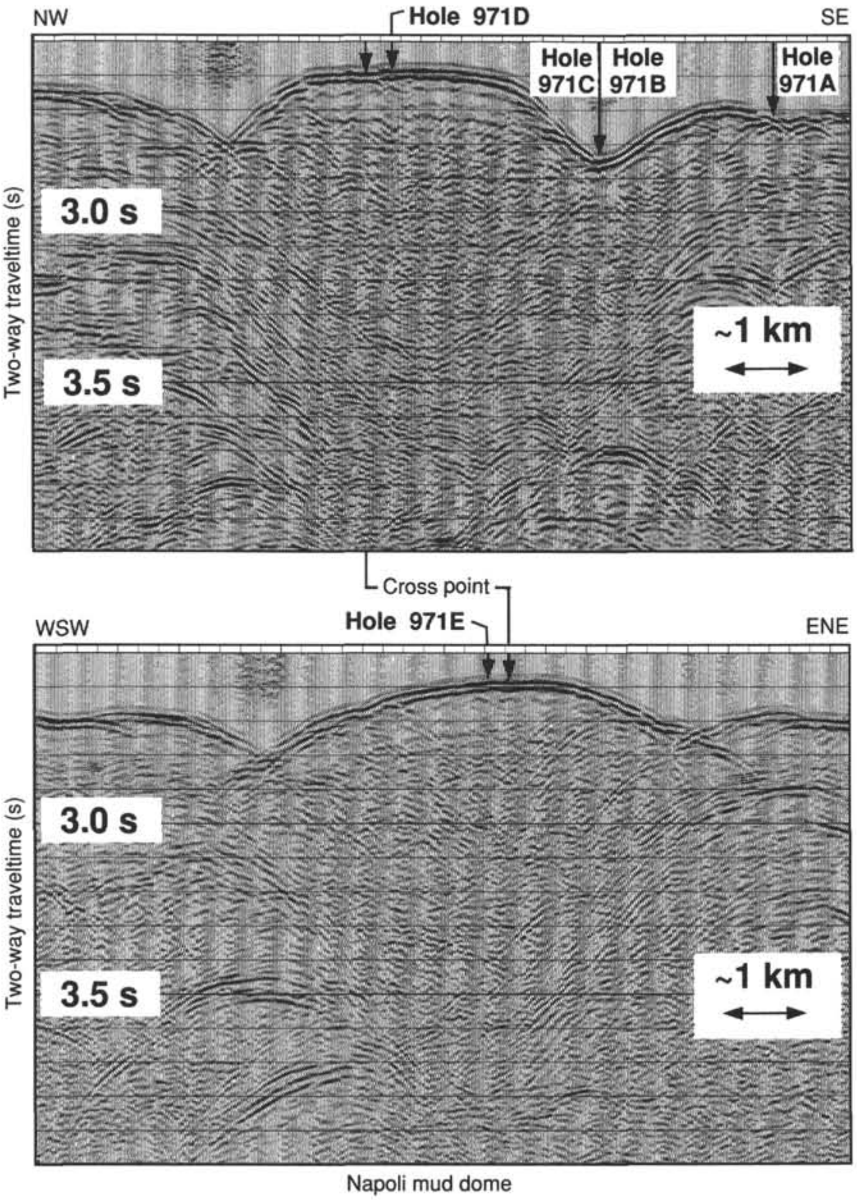

Figure 8. Seismic profile across the Napoli mud dome at Site 971. Horizontal lines are 100 ms TWT apart.

tary structure, petrographic observations on thin sections, and smear-slide composition. A lithostratigraphic summary of Site 971 is presented in Figure 9.

Unit I consists of light-colored intervals of nannofossil clay and nannofossil ooze with minor clayey nannofossil ooze, together with distinct dark-colored sapropels, which are composed of clay, nannofossil clay, and clay with nannofossils and foraminifers. All of these beds contain disseminated organic matter and pyrite with variable amounts of quartz, inorganic calcite, and plant fragments. One sapropel greater than 3 m in thickness (S5) was recovered from Holes 971B and 971C and contains a diverse assemblage of well-preserved diatoms.

Unit II consists of dark greenish-gray mudstone with highly variable quantities of clasts, nannofossils, clay, foraminifers, quartz, mica, and rock fragments. The textures observed allow the following subdivision of Unit II to be made:

Subunit IIA: matrix-supported clast-rich mud debris-flow deposits of dark gray silty clay to sandy silt-grade matrix with rounded to angular clasts varying in size from a few millimeters to tens of centimeters. Clasts are suspended within the mud without obvious sorting, and make up approximately 15%–35% of the core face.

Subunit IIB: mud debris-flow deposits consisting of a homogeneous, dark gray clay to silt-grade matrix supporting rare millimeter- to centimeter-sized mudstone clasts.

Subunit IIC: mousselike silty clay to sandy silt. The silty clay-grade matrix is interbedded with beds of silt to fine sand with gas vesicles. Scattered halite and carbonate clasts were found.

Description of Lithostratigraphic Units

Lithostratigraphic Unit I

Description: Nannofossil clay, nannofossil ooze, and clayey nannofossil ooze

Intervals: Cores 160-971A-1H and 2H, 10X through 12X, 160-971B-1H through Section 2H-5, and Cores 160-971C-1H and 2H

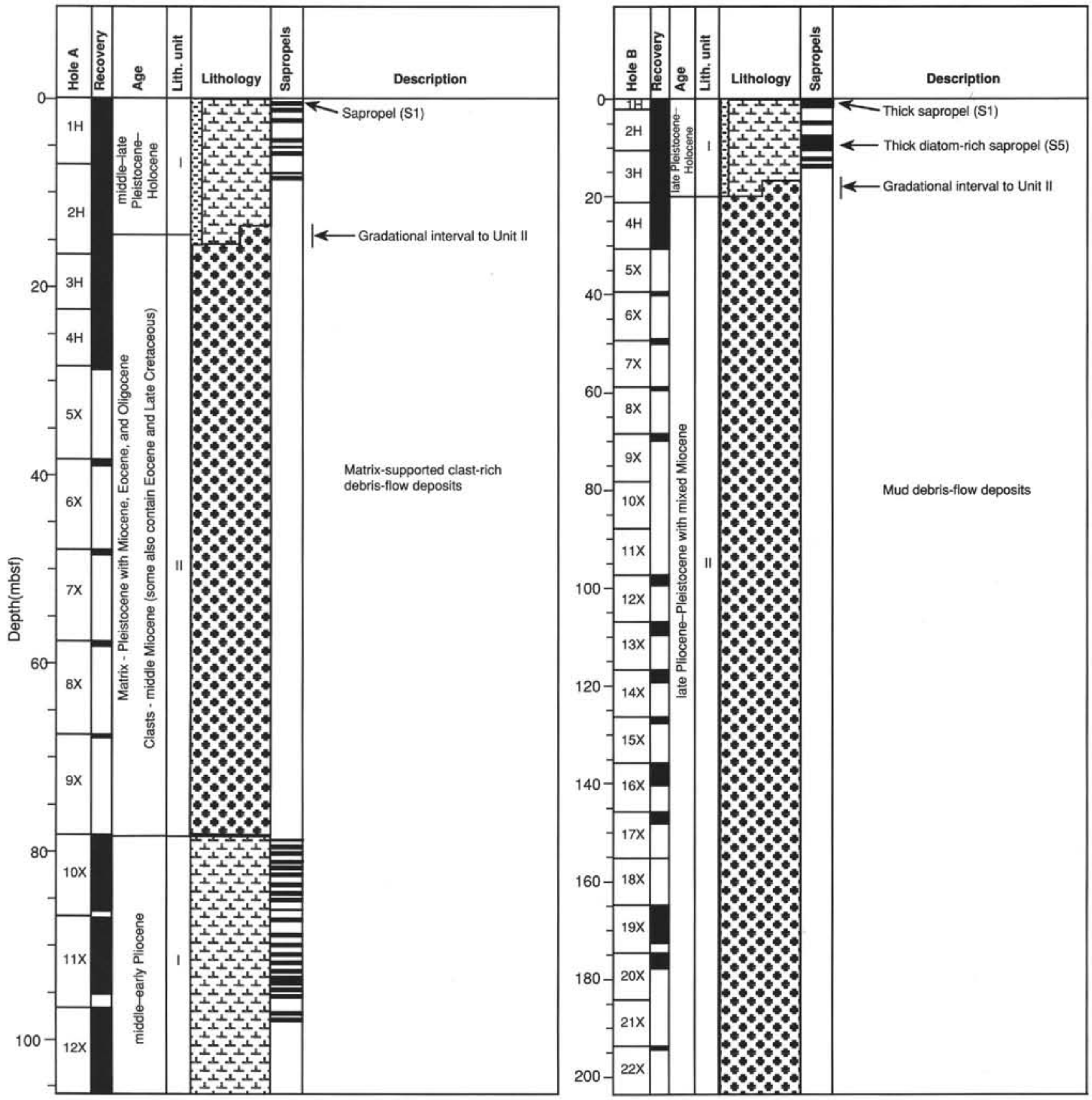

Figure 9. Core recovery, age information, and lithostratigraphic summary for Site 971.

Depth: 0–16.5 and 77–105.9 mbsf, Hole 971A; 0–20 mbsf, Hole 971B; 0–16.5 mbsf, Hole 971C
Age: late Pliocene to Holocene

The lithology of Unit I recovered in Holes 971A, 971B, and 971C is dominated by color-banded (decimeter to centimeter scale), moderately bioturbated light-grayish brown (10YR 5/2), light gray (10Y 6/1), gray (10Y 4/1), and greenish gray (5GY 5/1) nannofossil clay, nannofossil ooze, and clayey nannofossil ooze. Smear-slide analyses indicate that the sediment is composed of between 5% and 75% clay and between 20% and 80% nannofossils. Carbonate levels fluctuate between 4% and 68%, and the organic carbon content is between 0.1% and 0.6% (see "Organic Geochemistry" section, this chapter). Minor components include quartz, volcanic glass, and inorganic calcite.

Sapropels are between 1 and 330 cm thick and consist of dark gray (5Y 4/1), very dark gray (5Y 3/1), and black (5Y 2.5/1) clay, nannofossil clay, and clay with nannofossils and foraminifers. Minor components include disseminated amorphous organic matter and iron monosulfide with variable admixtures of quartz, inorganic calcite, and plant fragments. Volcanic glass is rare.

Turbidites of dominantly coarse silt layers with sharp basal contacts and fining-upward sequences are common at the base of the upper sequence of Unit I in Hole 971A (e.g., Sections 160-971A-2H-4 and 2H-5). A series of several millimeter- to decimeter-thick succes-

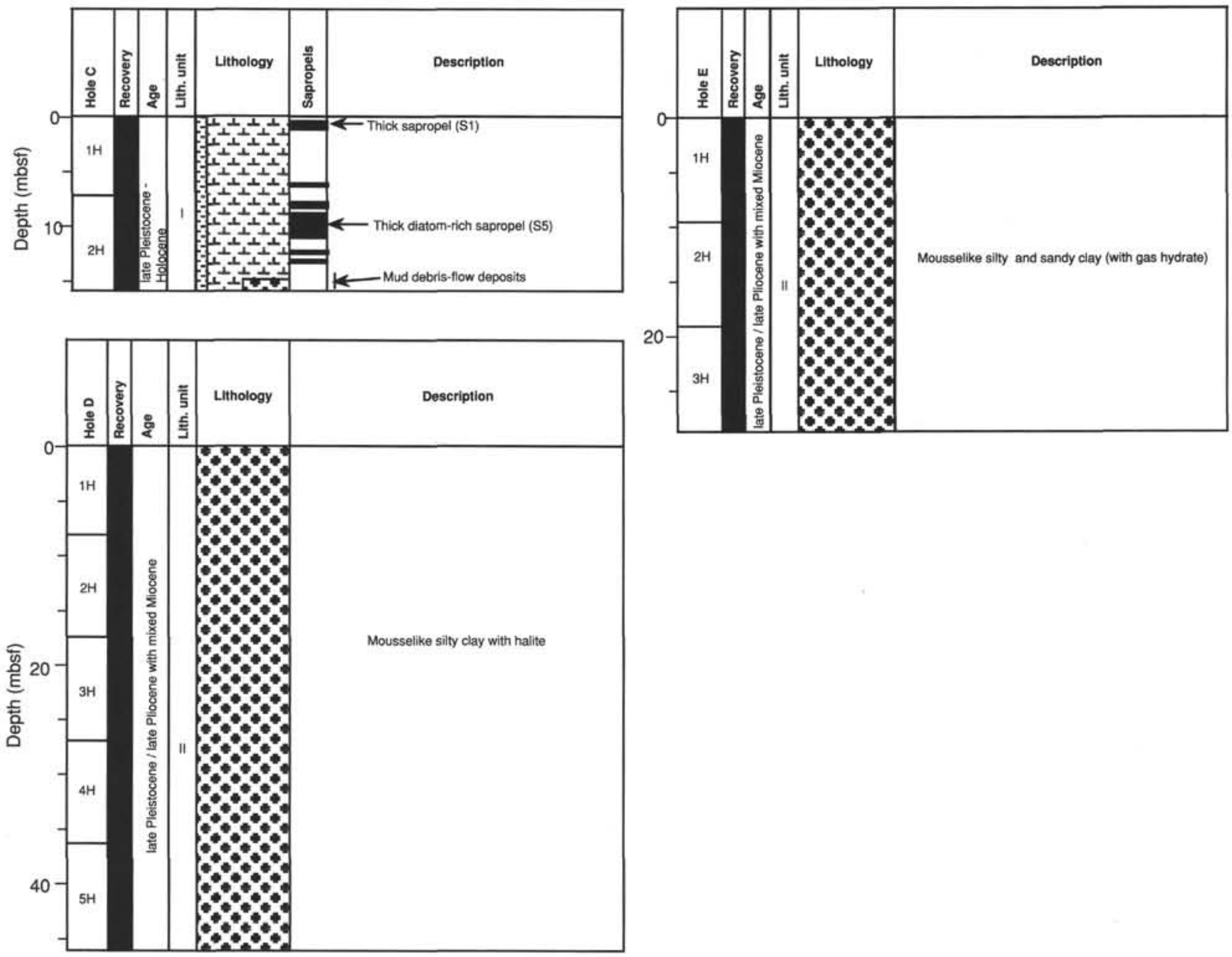

Figure 9 (continued).

sions (Fig. 10) may reflect a period of instability and gravity deposition resulting from a position on the slope beyond the moat (Fig. 11).

Sapropels

In the uppermost 17 m of upper Pleistocene to Holocene sediment in Hole 971A, 10 discrete sapropels were recognized. The upper nine beds (between 0 and 8.1 mbsf) correspond closely to the equivalent section cored in other Leg 160 sites, and S1, S3, S5, and S6 are all present in typical form. The lowermost sapropel, at 15.7 mbsf, is intercalated with multiple thin clay beds. All beds display sharp color contacts, and many contain burrow infills (*Chondrites*) that have partly destroyed lamination in some beds. The sequence recovered from Holes 971B and 971C is significantly thicker than the equivalent interval in Hole 971A (Fig. 12). Sapropel S1 (3% TOC) is expanded from 10 to 50 cm (Fig. 13), and the sequence to S6 is expanded from 5 m (Hole 971A) to 13.8 m (Hole 971B) and 13.2 m (Hole 971C). The ash layer above S3 is also thicker (10 cm in Hole 971A; 20 cm in Hole 971B). The most significant increase in thickness was observed in sapropel S5, which has an overall thickness of 3.3 m in Hole 971C with up to 6% TOC (Fig. 14). This bed is unique in that it comprises laminated diatom ooze with abundant and excellently preserved diatom frustules (see "Biostratigraphy" section, this chapter). Because Holes 971B and 971C are within a moatlike bathymetric depression at the base of the mud volcano (see "Geological Setting" section, this chapter), the enhanced thickness of the beds recovered from Holes 971B and 971C is attributed to increased sedimentation rates as a result of sediment ponding including localized resedimentation via debris-flow input and slumping (Fig. 15).

In the interval between 71 and 105.9 mbsf, 23 sapropels were recovered. These very dark gray (5Y 3/1) to black (5Y 2.5/1) sapropels are between 1 and 12 cm thick, display sharp color contacts, and are massive. They contain up to a maximum of 25% organic carbon (see "Organic Geochemistry" section, this chapter) and can be correlated with sapropels at other Leg 160 sites.

Lithostratigraphic Unit II

Description: Matrix-supported clast-rich mud debris-flow deposit, mud debris-flow deposit, mousselike silty clay to sandy silt
Intervals: Cores 160-971A-3H through 9X, Section 160-971B-3H-6 through Core 22X, Section 160-971C-2H-CC, Cores 160-971D-1H through 5H, and 160-971E-1H through 3H
Depth: 16.5–71 mbsf, Hole 971A; 20–203.5 mbsf, Hole 971B; 16.5–16.7 mbsf, Hole 971C; 0–46 mbsf, Hole 971D; 0–28.5 mbsf, Hole 971E
Age: Pleistocene

Lithostratigraphic Subunit IIA

Description: Matrix-supported clast-rich mud debris-flow deposits
Interval: Cores 160-971A-3H through 9X
Depth: 16.5–71 mbsf
Age: Pleistocene (1.5–0.46 Ma)

Subunit IIA was recovered only from Hole 971A. It consists of a dark gray, dominantly silty to clayey matrix with clasts of variable lithology, size, and shape (Table 2). Smear-slide analyses suggest that the principal components of the matrix are nannofossils, foramini-

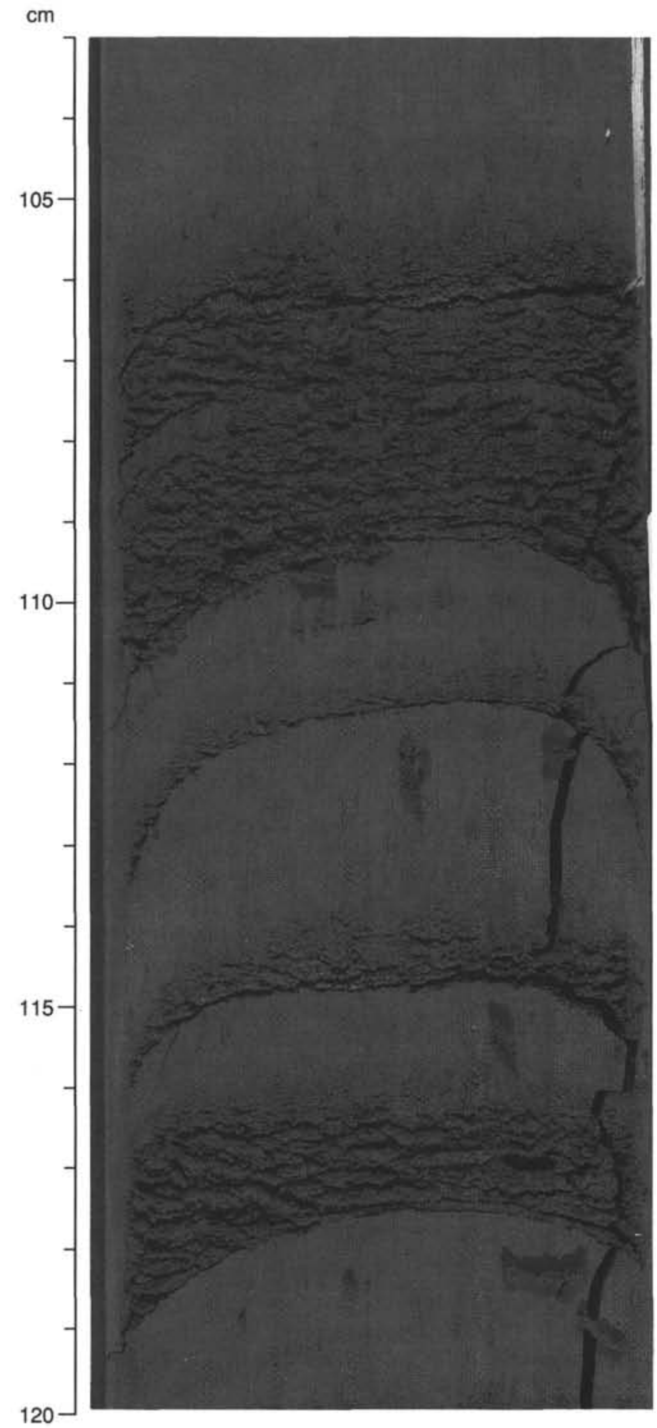

Figure 10. Example of thin silt beds fining upward to silty clay in Section 160-971A-2H-5, 103–120 cm.

fers, clay, quartz, and rock fragments. Minor quantities of dolomite and pyrite were also found (Table 3; see below). The upper boundary of the subunit is marked by a change in color from the light gray of the hemipelagic sediments (see above) to darker gray (5B 5/1) and by the appearance of clasts.

The textures and fabrics observed in this subunit are based upon the upper part of the interval (Cores 160-971A-3H and 4H), which had a recovery of 100% (cf., Fig. 9). Below Core 160-971A-4H, however, recovery averaged 10%. At the bottom of several of these short

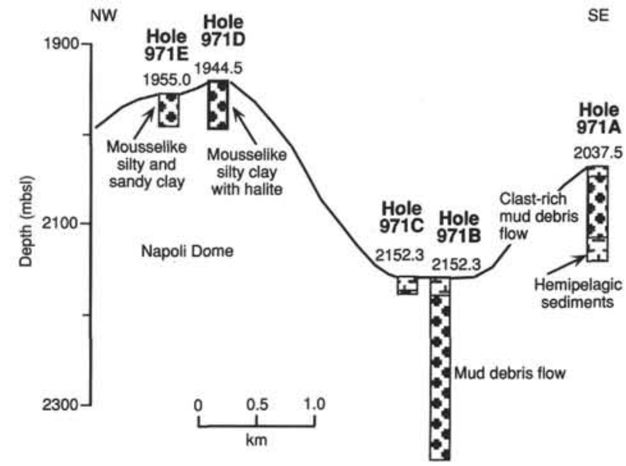

Figure 11. A cross section along the transect of holes drilled at Site 971 showing the debris-flow deposits (Unit II) interbedded with the hemipelagic succession recovered from Holes 971A, 971B, and 971C (Unit I). The cross section is drawn with reference to the seismic profile shown in Figure 8 (see "Site Geophysics" section, this chapter).

cores (e.g., Sections 160-971A-5X-CC, 6X-CC, 8X-CC, and 9X-CC) large lumps of well-lithified calcareous sandstone were recovered. These may represent fragments of larger clasts within the debris flow.

Clast size in the material recovered varies considerably, from a few millimeters up to greater than 100 mm in size (e.g., Section 160-971A-7X-1, 47–55 cm), but is dominantly gravel grade. The different clast types are summarized in Table 2 and discussed below. The morphology of the different clast types varies from angular to subrounded, but seems independent of composition, size, and degree of induration. No systematic variation of clast size or shape with depth was observed.

Estimates of the clast:matrix ratio suggest that there is no obvious variation in clast abundance throughout the entire section in Hole 971A (Fig. 16). The maximum clast size shows a scatter between 12 and 50 mm where recovery was good. Higher values with a greater range in size were recorded in intervals where recovery dropped (Fig. 16). A representative example for sedimentary texture of the clast-rich mud debris-flow deposits shows a clast:matrix ratio of about 3:7 (Fig. 17).

Layerlike features within both the clast-rich interval (e.g., Sections 160-971A-3H-2 and 3H-3) and the more homogeneous mud flow (up to 3-cm-thick bands of light gray nannofossil clay) indicate that the sequence contains bedding. In Section 160-971A-7X-1, 14–34 cm, a unique sequence of interbedded bluish gray (5B 4/1) and reddish brown (5YR 5/3) mudstones was found (Fig. 18). On a millimeter to centimeter scale, clast-supported gravel-sized beds with maximum clast sizes less than 10 mm across are intercalated with millimeter-thick laminae of dark greenish gray silt. Both the blue and red mudstones are highly variable in grain size (silt to gravel grade) and either form separate layers or are mixed. The mudstone clasts are dominantly angular to subrounded.

The absence of carbonate in these mudstones, in contrast with the predominance of calcareous mudstones observed throughout the entire subunit, implies that the layers have a different source than the majority of clasts. One possibility is that the layers represent local postdepositional reworking of individual larger debris-flow clasts. Small (<5 mm) clasts of both the blue and red mudstones occur scattered sparsely through the sediment matrix above and below the color-laminated sequence (Cores 160-971A-5X through 9X).

Both the upper and lower bases of the matrix-supported clast-rich mud debris flows were penetrated in Hole 971A; however, the contact between the hemipelagic sediments of Unit I and Subunit IIA lies

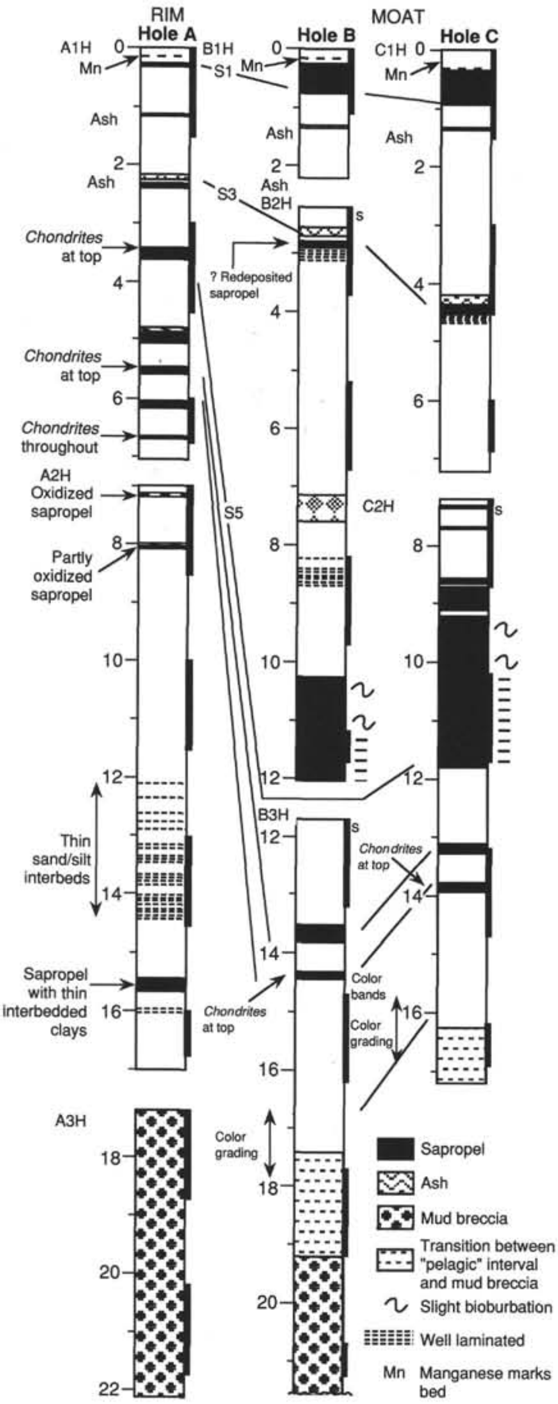

Figure 12. Interhole correlation of upper Pleistocene–Holocene sapropels from Holes 971A, 971B, and 971C. The extended thickness of the sequence in Holes 971B and 971C might be the result of sediment ponding in the moatlike depression at the base of the Napoli mud volcano.

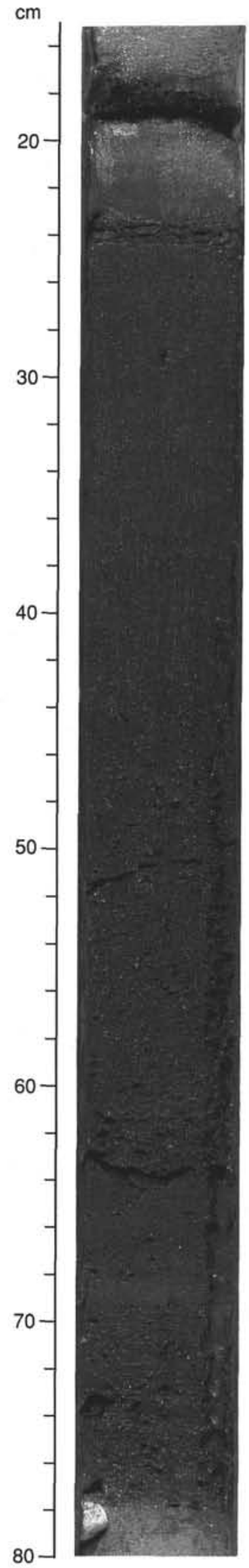

Figure 13. Example of the extended sapropel S1 layer in Section 160-971B-1H-1, 15–80 cm.

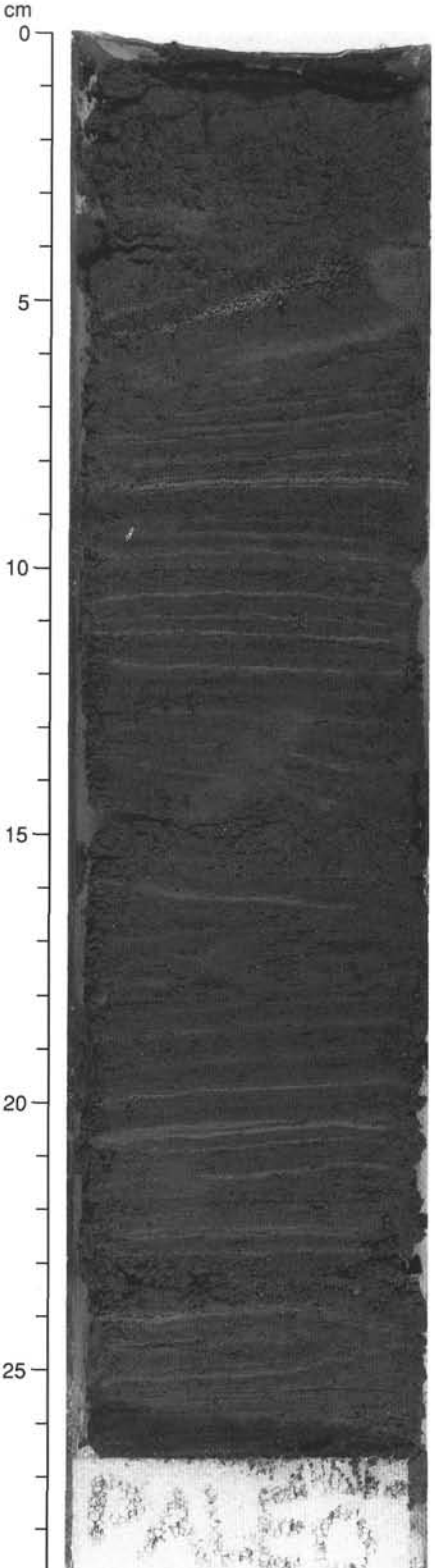

Figure 14. Example of an interval within sapropel S5 in Section 160-971B-2H-CC, 0–29 cm. The sapropel is expanded (total thickness of 183 cm) compared to its occurrence in Hole 971A and characterized by a significant abundance of diatoms and distinct laminations on a millimeter scale.

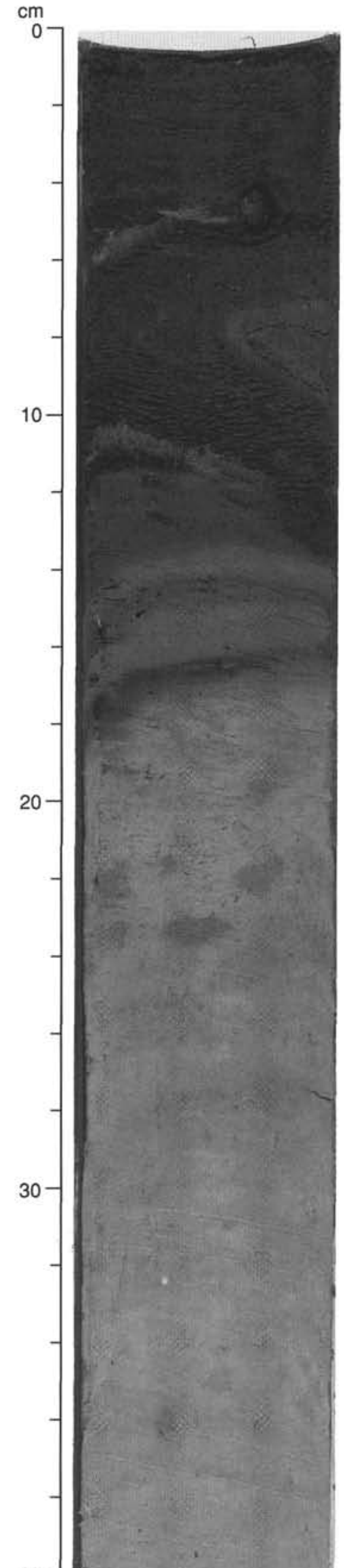

Figure 15. Slump fold at the base of a sapropel in Section 160-971C-2H-4, 0–40 cm. The trace of the folded bedding planes is well imaged by a millimeter-thick light gray band of nannofossil clay.

Table 2. Major clast characteristics at Site 971.

Lithology	Size (mm)	Color	Grain size, sorting	Shape	Carbonate content	Lithification	Hole, core, section, interval (cm)	Comments
Claystone, mudstone	35	Black to dark greenish-gray	Clay size, homogeneous	Angular to subrounded	Noncalcareous	Semiconsolidated	971A-4H-3, 60–63	Homogeneous, some fissility
Claystone, mudstone	7	Reddish and bluish	Clay size, homogeneous	Subangular to subrounded	Noncalcareous	Semiconsolidated	971A-7X-1, 20–21	Interbedded
Claystone, mudstone	80	Light greenish gray	Very fine	Subangular to subrounded	Calcareous	Unconsolidated	971A-6X-1, 32–38	Homogeneous
Claystone, mudstone	34	Dark greenish gray	Very fine	Subangular to subrounded	Calcareous	Semiconsolidated	971A-6X-CC, 20–23	Homogeneous
Pelagic limestone	15	Middle gray (N4)	Fine silt to sand, poorly sorted	Angular to subangular	Calcareous	Well lithified	971E-1H-1, 136–138	Foraminifer-bearing, mollusk shells
Siltstone	64	Greenish gray (5GY 4/1)	Well sorted	Subrounded	Calcareous	Well consolidated	971A-4H-2, 110–117	
Siltstone	50	Greenish gray	Well sorted	Subrounded	Calcareous	Semiconsolidated	971B-16X-3, 12–17	Interbedded
Sandstone	53	Dark gray	Very coarse grained	Subrounded	Calcareous	Poorly lithified	971A-5X-CC, 31–36	
Sandstone	33	Brownish gray	Fine sand	Subangular	Calcareous	Poorly lithified	971A-4H-1, 70–73	
Sandstone	152	Greenish gray	Medium sand, well sorted	Rounded to subangular	Calcareous	Semilithified	971A-5X-CC, 10–25	Quartz, feldspar, mica, opaque minerals, glauconite, benthic and planktonic foraminifers; lamination discernable

Table 3. Smear-slide data (%) for the dominant lithology (i.e., matrix) of selected sections at Site 971.

Core, section, interval (cm)	Depth (mbsf)	Clay	Nannofossils	Foraminifers	Quartz	Feldspar	Volcanic glass	Inorganic calcite	Dolomite	Rock fragments	Opaque minerals	Diatoms	Organic debris
160-971A-													
1H-3, 80–81	3.8	40	46	0	3	0	0	5	2	0	2	0	0
2H-3, 74–75	10.74	17	54	6	3	3	1	5	2	1	0	0	0
2H-7, 50–51	16.5	10	65	8	2	0	0	5	2	5	2	0	0
3H-1, 50–51	17	64	14	2	5	0	0	2	2	9	2	0	0
4H-1, 21–22	22.71	45	10	9	5	3	0	21	0	18	2	0	0
4H-1, 44–45	22.94	67	15	0	7	4	0	2	1	2	2	0	0
5X-CC, 27–28	28.77	68	16	0	2	2	0	0	0	10	2	0	0
10X-1, 84–85	77.84	4	80	5	2	1	1	4	2	0	1	0	0
10X-3, 37–38	80.37	4	79	8	1	1	2	2	2	0	1	0	0
10X-6, 15–16	84.65	23	60	9	1	0	2	2	1	0	0	0	0
11X-1, 97–98	87.67	42	38	9	2	0	2	3	1	0	1	0	0
11X-4, 70–71	91.9	24	64	6	2	0	1	2	0	0	1	0	0
12X-3, 73–74	100.03	36	49	11	1	0	0	2	1	0	0	0	0
12X-4, 133–134	102.13	6	83	4	1	0	2	2	0	0	0	0	0
160-971B-													
2H-1, 80–81	3	23	53	10	2	1	0	7	2	0	0	0	0
2H-5, 80–81	9	33	52	5	1	0	2	4	1	1	0	0	0
3H-6, 80–81	20	50	13	2	2	1	1	2	9	14	6	0	0
3H-6, 88–89	20.08	45	20	1	4	2	1	2	10	12	8	0	0
4H-4, 100–101	26.7	78	8	1	1	1	1	1	4	2	2	0	0
14X-1, 30–31	117	62	22	0	2	1	1	2	1	8	1	0	0
14X-1, 70–71	117.4	72	14	0	2	0	0	2	1	9	0	0	0
14X-2, 30–31	118.5	51	9	6	13	3	0	0	0	10	3	0	0
19X-3, 60–61	168.5	47	3	13	15	0	1	3	2	13	0	0	0
160-971C-													
2H-1, 80–81	8	76	14	3	1	0	0	4	1	0	1	0	0
2H-2, 65–66	9.35	15	2	6	1	0	0	2	0	0	1	60	6
2H-3, 91–92	11.11	18	3	0	2	0	0	0	0	0	2	72	1
2H-3, 110–111	11.3	16	5	5	0	0	0	1	5	1	2	60	2
2H-3, 140–141	11.6	16	0	2	1	0	0	2	2	0	4	67	2
2H-5, 10–11	13.3	13	60	12	1	0	0	5	0	0	5	0	3
2H-7, 40–41	16.6	40	26	8	3	0	1	2	6	8	6	0	0
160-971D-													
1H-2, 50–51	2	45	30	0	4	0	0	6	4	4	7	0	0
1H-5, 4–5	6.04	47	6	5	9	0	0	2	9	14	8	0	0
2H-2, 50–51	10	55	25	0	1	0	0	2	5	2	10	0	0
3H-3, 80–81	21.3	65	12	0	5	0	0	5	3	2	8	0	0
4H-3, 40–41	30.4	52	20	0	0	0	0	6	8	4	8	0	0

between Cores 160-971A-2H and 3H and 9X and 10X, respectively, and was not recovered.

Lithostratigraphic Subunit IIB

Description: Mud debris-flow deposits
Intervals: Section 160-971B-3H-6 through Core 22X and Section 160-971C-2H-CC
Depth: 20–203.5 mbsf, Hole 971B; 16.5–16.7 mbsf, Hole 971C
Age: Pleistocene–?

Subunit IIB was recovered from two holes drilled at the foot of the Napoli mud volcano in a moatlike feature (Fig. 11). The top of Subunit IIB is identified by a distinct change to a darker gray color (5Y 3/1) in both Holes 971B and 971C from the brownish to dark greenish gray color (5BG 6/1 to 5GY 4/1) of the sapropel-bearing sediments. This change occurs at the very base of Core 160-971C-2H, and is followed by an interval with up to 15% clasts.

Sediments of Subunit IIB consist of dark greenish gray (5B 5/1 to 5GY 4/1) homogeneous silty clay to clay. Smear-slide analyses sug-

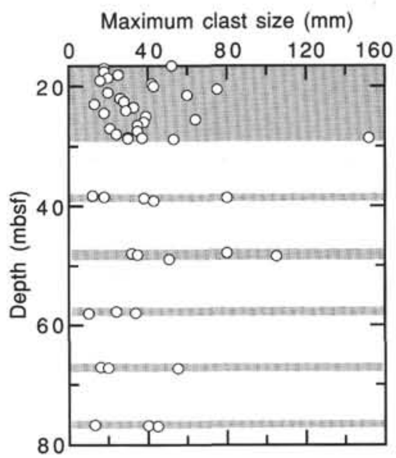

Figure 16. Maximum clast size vs. depth for matrix-supported clast-rich mud debris flows of Subunit IIA. Shaded areas indicate core recovery. See the text for discussion.

gest that clay content varies from 45% to 78% (Table 2). The percentage of nannofossils varies from 3% to 22%. Rare, poorly consolidated to well-indurated mudstone clasts are scattered through these sediments. Subtle changes in grain size indicate that this unit is, at least in part, a bedded succession with silt to fine-sand beds reaching up to 40 cm in thickness (e.g., Section 160-971B-4H-3). Sand patches (1–10 cm across) have no apparent systematic orientation related to these bedding fabrics, but usually occur adjacent to silt-rich intervals. Intervals of clast concentration (up to 30%; cf., Sections 160-971B-4H-3 through 4H-CC) are generally dominated by mudstone. However, between Cores 160-971B-16X and 17X is a zone containing abundant limestone as well as mudstone clasts. Clasts also occur more commonly toward the bottom of the hole (Sections 160-971B-20X-CC and 22X-CC) (Fig. 19). Below 180 mbsf, core recovery dropped significantly to less than 5%–10%, and well-lithified calcareous sandstone and calcareous mudstone clasts up to 65 mm long were recovered.

Lithostratigraphic Subunit IIC

Description: Mousselike silty clay to sandy silt
Intervals: Cores 160-971D-1H through 5H and 160-971E-1H through 3H
Depth: 0–46 mbsf, Hole 971D; 0–28.5 mbsf, Hole 971E
Age: ? (both late Pleistocene and middle Miocene, reworked?)

Sediments of both Holes 971D and 971E in the crestal area of the Napoli Dome were classified as Subunit IIC on the basis of their texture, which is characterized by an abundance of small gas vesicles (Fig. 20). The sediment is dark gray to dark green in color (N5 to 5GY 4/1) and composed of a clay- to silt-grade matrix with several intercalated coarser intervals. In previous studies on comparable material, this texture is described as mousselike (e.g., "Lithostratigraphy" section, "Site 970" chapter, this volume; Camerlenghi et al., 1992; Staffini et al., 1993) and is thought to be caused by the presence of a solid phase released as a gas during drilling (e.g., Westbrook, Carson, Musgrave, et al., 1994). All the cores recovered from Hole 971D displayed the mousselike fabric together with distinct gaps perpendicular to the core axis, which are also thought to be caused by gas expansion (up to >20 cm per section). Sediment recovery at Hole 971E was associated with a strong odor and the loss of >5 m of sediment caused by gas expansion.

Bedding planes are clearly evident in the mud volcano deposits recovered from Holes 971D and 971E. Throughout both successions, cycles of sand or silt beds grade upward to clayey silt over a few centimeters (Fig. 20).

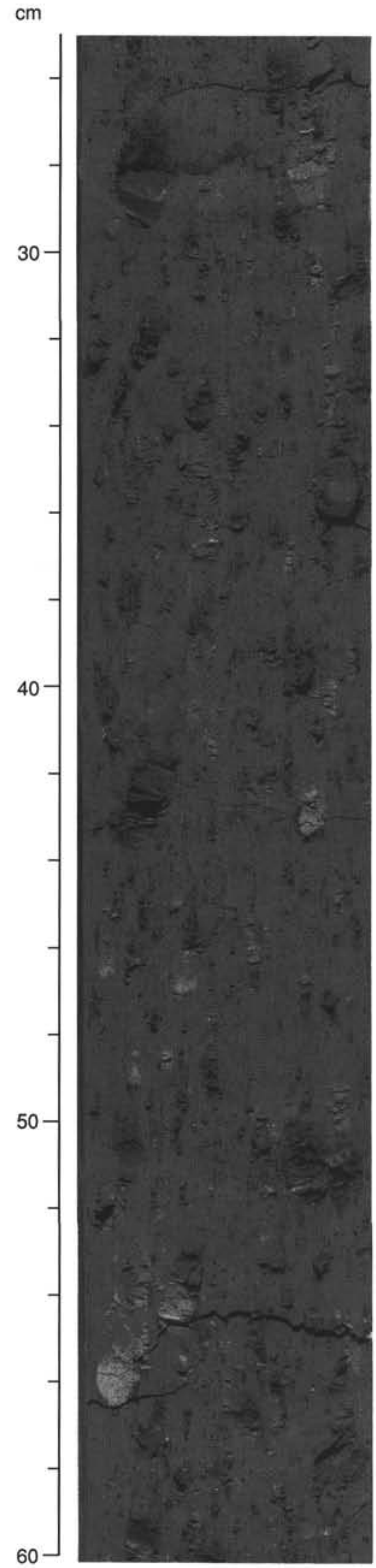

Figure 17. Example of fabrics of matrix-supported clast-rich mud debris flows from Section 160-971A-3H-2, 25–60 cm. In this interval, semiconsolidated mudstone clasts reach an abundance of about 15%.

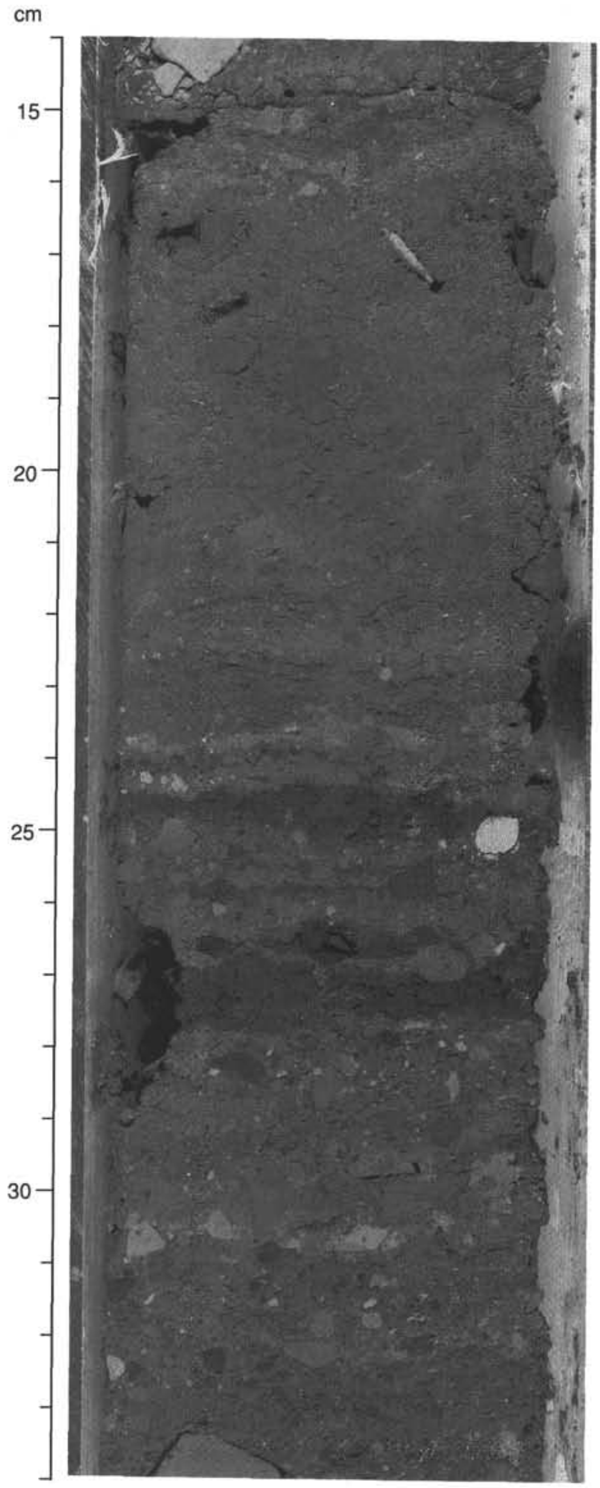

Figure 18. Layered redeposited claystone beds recovered at Section 160-971A-7X-1, 14–34 cm. For description and interpretation, see text.

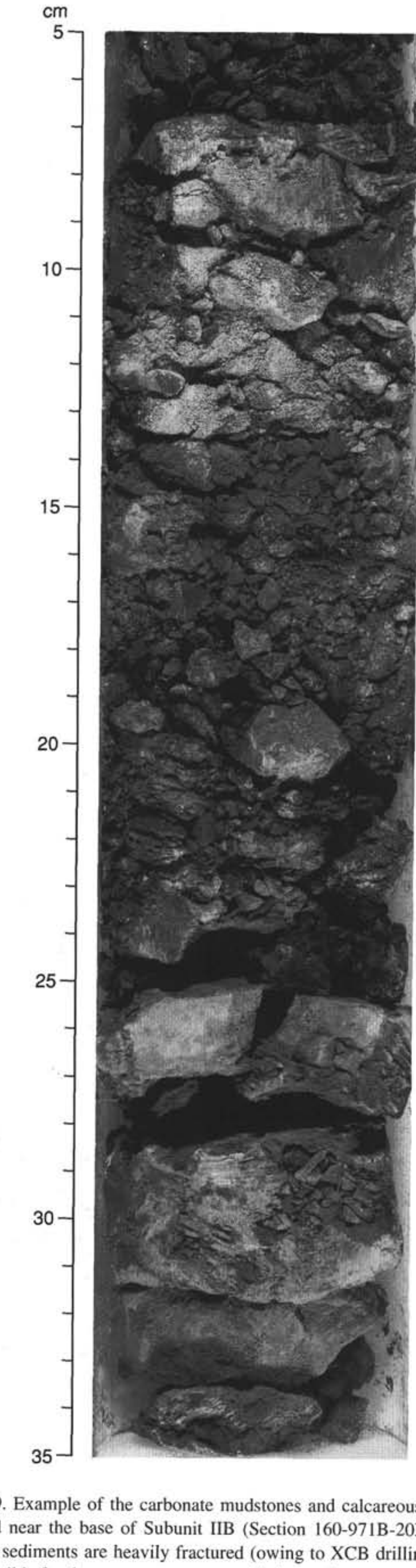

Figure 19. Example of the carbonate mudstones and calcareous sandstones recovered near the base of Subunit IIB (Section 160-971B-20X-CC, 5–35 cm). The sediments are heavily fractured (owing to XCB drilling) and may be responsible for the poor recovery over this interval.

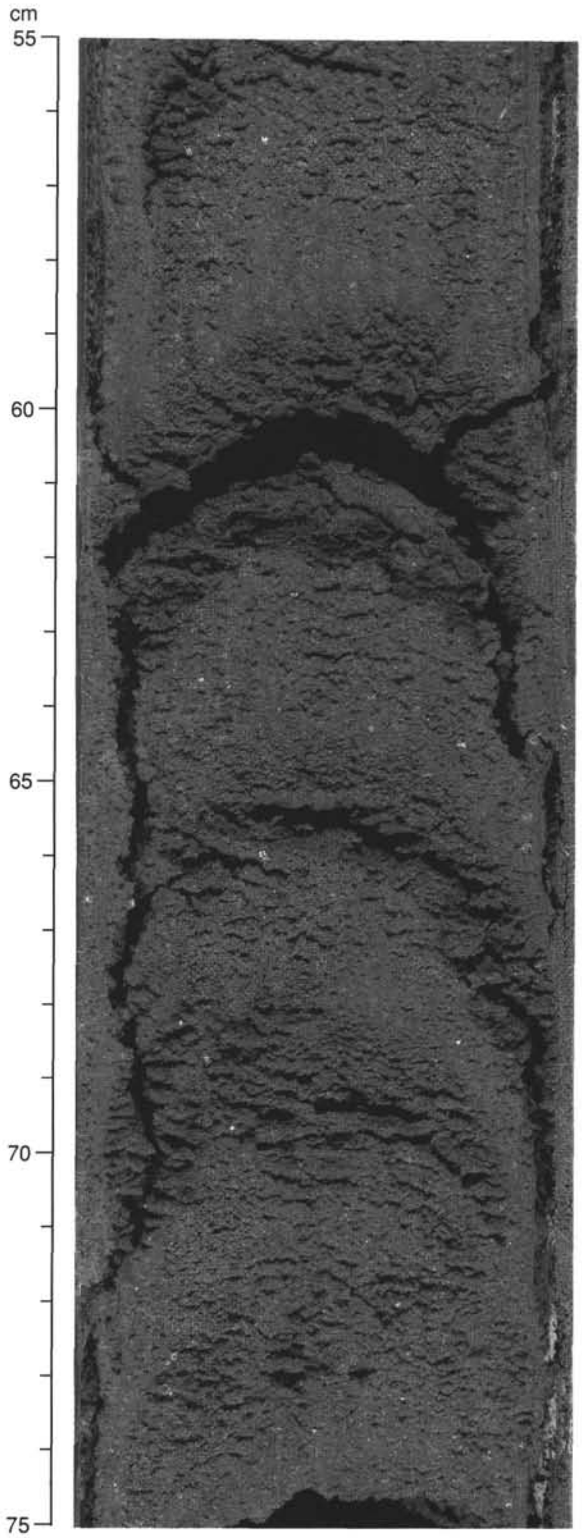

Figure 20. Silt bands in mousselike silty clay at Section 160-971D-2H-2, 55–75 cm. The silts show upward-fining cycles on a centimeter scale.

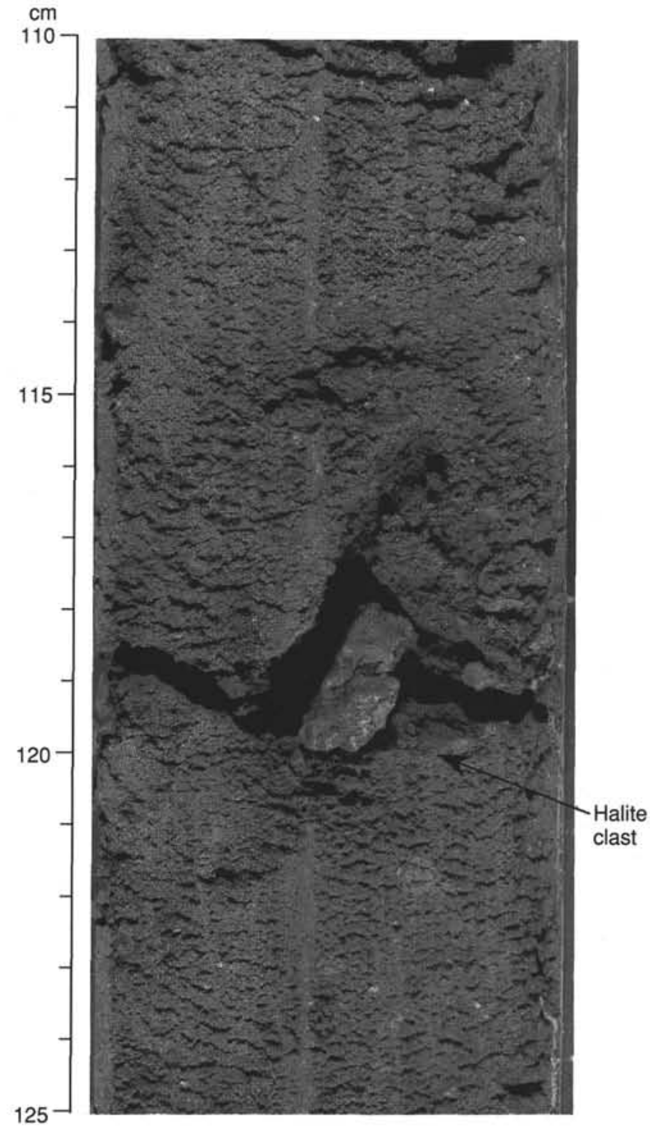

Figure 21. Clast of crystallized halite in mousselike silty clay at Section 160-971D-4H-1, 110–125 cm. The disturbance of the texture around the clast is thought to be induced by either drilling or the cutting process rather than the precipitation of halite.

Although pore waters from all holes drilled at Site 971 were saturated with halite (see "Inorganic Geochemistry" section, this chapter), solid-phase salt was found only in Hole 971D (Fig. 21). Another indication of the abnormally high salinity in this hole was the precipitation of halite on the core face while on the description table. Crystals up to 0.5 cm across were found within vesicles. Besides pure halite clasts and halite-cemented conglomerate clasts (see Fig. 21 and below), mud clasts and mudstones are scattered sparsely throughout.

Clast Description

Most of the clast types recovered in the mud-debris flows are common to all three subunits recovered at Site 971, although much higher abundances were found in Subunit IIA (matrix-supported clast-rich mud debris-flow deposits). Clast lithologies present in each of the subunits fall into four groups: mudstone, sandstone, siltstone, and several carbonate rocks. The mudstones vary from almost unconsolidated to partly lithified and are both calcareous and noncalcareous. Mudstones are the dominant clast lithology throughout.

The sandstones contain a mixed grain population indicating multiple sources including metamorphic rocks (micaceous schist, metacarbonate, quartzite), plutonic igneous rocks, and sedimentary rocks (Table 2). Faunal evidence from some of the calcareous mudstone and carbonate clasts also suggests that reworking of Eocene and Cretaceous sediment occurred during the Miocene (see "Biostratigraphy" section, this chapter). Planktonic foraminiferal micrite clasts of early to middle Miocene age suggest relatively deep-water accumulation at this time (see "Biostratigraphy" section, this chapter). The presence of pelagic chalk with foraminifers and mollusk shells supports this hypothesis (Table 2). Early Miocene (Burdigalian to Langhian) age clasts appear to dominate the succession, but younger (middle Miocene to Pleistocene) material was also found (see "Biostratigraphy" section, this chapter).

Two types of halite-bearing clasts were found within the succession of mousselike muds of Hole 971D. Coarse-grained (up to 4 cm) amalgamated halite crystals with irregular shapes are scattered through the matrix and enriched in Cores 160-971D-4H and 5H (e.g., Fig. 21). In some places (e.g., Section 160-971D-5H-6, 116–118 cm) clasts consisting of aggregates of pebbles are cemented with halite. These 5 × 8 mm pebbles are subrounded to rounded mud clasts of varying colors. Some of the mudstone clasts contain millimeter-sized mud clasts, indicating some earlier stage of reworking and/or redeposition. Evidence of in situ precipitation of halite and the resulting fabric distortion that would ensue is limited. Both types of halite-bearing clasts are therefore believed to have formed at deeper levels within the sedimentary succession and been transported upward as clasts.

Although the majority of the clasts are subangular to subrounded in shape, both angular and rounded examples of all lithologies were observed. This suggests that there is not a simple relationship between clast lithology and angularity.

Matrix

Both the initial visual core description and smear-slide analyses indicate that the matrix composition varies both within and among the subunits at Site 971. The matrix is dominantly silty clay with nannofossils in Subunits IIA and IIB, but there is a significant increase in average grain size in the holes drilled at the crest the Napoli mud dome. The matrix with the mousselike texture in Holes 971D and 971E is mainly clayey silt (interbedded with medium silt) to silt (interbedded with sandy silt to fine sand). Quartz, foraminifers, dolomite, and rock fragments are common in several samples from all holes (see Table 3).

Structural Information

Measurement of structures was conducted only on the pelagic sedimentary sequences of Unit I, for which the data are listed in Table 4. Almost all the bedding and fault information were obtained from the upper part of Holes 971A and 971B, where the bedded nature of the sediment was not affected by XCB coring. Both bedding planes and faults were measured relative to the core coordinate system. Tensor data were not available for this site, so the structural measurements cannot be corrected to geographic coordinates.

Horizontal to subhorizontal sedimentary bedding was found throughout the layered hemipelagic succession at Holes 971A, 971B, and 971C. Slight to moderate tilting of the bedding planes (mainly 5°–15°; cf., Table 4) is common in Hole 971A, with increasing inclination downhole in Hole 971B.

Irregular sedimentary contacts, found at several intervals in the deeper sequence recovered from Hole 971A (e.g., Cores 160-971A-10X through 12X), are thought to be the result of slight scour on the base of debris flows. Many of these may have been induced by XCB drilling.

Only sporadic small-scale normal faulting was found in the hemipelagic sediments recovered from this site (e.g., Sections 160-971A-1H-5 and 2H-1). Steeply dipping fault planes (at about 70°) show offsets of 0.1 cm to more than 20 cm.

Summary and Interpretation

In summary, the following points permit an initial interpretation of deposition of the Napoli mud volcano sediments:

1. A period of hemipelagic sedimentation occurred in the early to late Pleistocene, resulting in the deposition of a sapropel-bearing succession (S1 to S7; see Figs. 9, 12).
2. Significant thickening of time-equivalent intervals is visible in Holes 971B and 971C in the moatlike feature relative to Hole 971A on a topographic rise away from the volcano.
3. Sapropel S5, which is thickened in Holes 971B (>3 m) and 971C, contains a well-preserved assemblage of diatoms.
4. Different types of sedimentary textures were found in each of the five holes drilled along the Napoli Dome transect.
5. Mud debris-flow deposits rich in clasts (Subunit IIA) reflect an earlier stage of extrusive activity (1.5–0.46 Ma; see "Biostratigraphy" section, this chapter) than the more homogeneous sediments with fewer clasts (Subunit IIB) that were recovered at a higher stratigraphic level (older than 0.26 Ma; see "Biostratigraphy" section, this chapter). This observation is in agreement with the results from Site 970 (Milano mud volcano, see "Lithostratigraphy" section, "Site 970" chapter, this volume), where clast-rich material appears to represent an earlier stage of mud volcano activity.
6. Mousselike silty clay to silt with abundant gas vesicles was recovered from Holes 971D and 971E in the crestal area of the Napoli Dome.
7. Subunits IIA and IIB appear to interfinger with the hemipelagic sediments of Unit I in Holes 971A, 971B, and 971C.
8. A similar range of heterogeneous clast types was found throughout all subunits. They comprise calcareous and noncalcareous mudstones, siltstones, and sandstones. Rare halite, conglomerate (Hole 971D), and pelagic chalk clasts (Hole 971E) were identified.
9. There is evidence for both sedimentary layering and grading within the mud breccia subunits. On the basis of these observations, an intrusive mechanism of sedimentation is unlikely.
10. No systematic relation between clast type and lithification, size, or shape could be found. The relationship between clast types and their depth of occurrence has not been fully investigated.

BIOSTRATIGRAPHY

Calcareous Nannofossils

Hole 971A

Hole 971A was drilled into the eastern flank of the Napoli mud volcano. Two general lithologies and modes of deposition were interpreted from the Hole 971A data. Correspondingly, the paleontological data collected from this site reflect the two different lithologies. The first lithology occurs in the upper 20 m of the hole and consists of pelagic sediments with abundant in situ nannofossil assemblages and only minor reworked material. The second lithology consists of clast-rich mud debris-flow deposits containing primarily middle Miocene nannofossil assemblages with minor amounts of Pleistocene

Table 4. Structural data collected at Site 971.

				Orientation on core face (degrees)		Second apparent orientation (degrees)		Calculated orientation (degrees)		
Core, section, interval (cm)	Depth (mbsf)	Feature	Offset (cm)	Apparent dip	Direction	Apparent dip	Direction	Dip	Direction	Comments
160-971A-										
1H-1, 26	0.26	SB		2	90	9	180	9	168	Top of sapropel
1H-2, 81	2.31	SB		5	270	12	0	13	338	Yellow band
1H-2, 84	2.34	SB		0	90	2	180	2	180	Top of sapropel
1H-3, 38	3.38	SB		2	270	24	0	24	356	Purple band (geochemical front?)
1H-3, 42	3.42	SB		0	90	0	0	0	90	Top of sapropel
1H-5, 43–61	6.43	F	0.1	68	270	0	354	68	264	Normal
1H-5, 50	6.50	SB		2	270	4	180	4	207	Geochemical front
2H-1, 61–77	7.61	F	>20	65	270	0	45	72	315	Normal curviplanar fault
2H-2, 62–63	9.12	SB		15	90	7	180	16	145	Sand layer
2H-3, 142	11.42	SB		9	90	17	0	19	27	Sand layer
2H-4, 90–93	12.40	SB/DI		28	90	16	0	31	62	Sand layer
2H-4, 148–149	12.98	SB/DI		12	90	22	0	25	28	Sand layer
2H-7, 17–20	16.17	SB		13	90	18	0	22	35	Sand layer
10X-2, 40–240	78.90	SB		0	90	0	180	0	90	Ash
10X-2, 114–117	79.64	DIS/DI		25	90	11	0	27	67	
10X-5, 90	83.90	SB		5	270	3	0	6	301	Ash
10X-5, 95–100	83.95	F		38	270	10	0	39	283	
160-971B-										
2H-1, 37	2.57	SB		17	90	20	0	25	40	Base of turbidite
2H-1, 106	3.26	SB		11	90	4	180	12	110	Base of turbidite
2H-2, 100	4.70	SB		0	90	5	180	5	180	Silt band
2H-5, 16–17	8.36	SB		17	270	4	0	17	283	Top of sapropel
3H-2, 58–59	13.78	SB		7	270	6	0	9	311	Base of sapropel
3H-3, 6–7	14.76	SB		4	270	5	0	6	321	Foraminifer sand
3H-4, 8–13	16.28	SB		33	270	32	0	42	314	Clay
3H-5, 94–103	18.64	SB		55	270	4	0	55	273	Transition zone
3H-5, 121–130	18.91	SB		46	270	30	0	50	299	Transition zone
3H-6, 130–135	20.50	SB		36	90	14	180	38	109	Boundary between clay and clast-rich layer
3H-6, 137–142	20.57	SB		45	270	37	0	51	307	

Note: Feature symbols defined in Table 2 ("Explanatory Notes" chapter, this volume).

taxa (Fig. 22). Unlike the sediments recovered at Site 970, where intercalations of pelagic intervals provided age control on the mud breccia, the exact timing of the emplacement or redeposition of the mud breccia is difficult to establish owing to a paucity of in situ nannofossils. The problem of Pleistocene age control is most difficult in the lower portion of the hole, where Pleistocene specimens are particularly rare or absent.

Calcareous nannofossils were studied principally from core-catcher samples. Additional samples were collected from the uppermost three cores where zonal boundaries were believed to occur. Numerous clasts were also collected from within the mud breccia and analyzed.

Pelagic sediments from Cores 160-971A-1H and 2H range from Zones MNN21a to MNN20, which indicates deposition in the late to middle Pleistocene. The nannofossils are affected by dissolution and overgrowths, which hinder the identification of small fragile taxa such as *Emiliania huxleyi*. *E. huxleyi* fluctuates from rare to common in Samples 160-971A-1H-1, 80 cm, through 1H-5, 40 cm. Positive identification of *E. huxleyi* using a scanning electron microscope during post-cruise studies is warranted for this interval of limited preservation. The accompanying assemblage includes small *Gephyrocapsa* (<3.5 μm), *Gephyrocapsa oceanica* s.l., *Helicosphaera kamptneri, Coccolithus pelagicus, Rhabdosphaera clavigera,* and *Pontosphaera japonica.* There is little or no reworking evident.

From Cores 160-971A-3H through 9X, a fine-grained breccia that contains predominately middle Miocene nannofossils was recovered. Preservation and abundance of in situ Pleistocene nannofossils and reworking vary throughout the breccia. From Samples 160-971A-1H-CC through 2H-5, 127 cm, the assemblage lacks both *E. huxleyi* and *Pseudoemiliania lacunosa.* These samples were therefore placed into the gap Zone MNN20. From Samples 160-971A-2H-6, 133 cm, through 2H-CC, *P. lacunosa* is present and indicates that these samples are within Zone MNN19f. Variable quantities of Late Cretaceous, middle Miocene, Eocene and maybe early Oligocene age taxa are evidenced by the presence of *Ericsonia formosa, Helicosphaera walberdorfensis, Sphenolithus predistentus, Micula decussata, Eiffellithus* sp., *Reticulofenestra umbilica, Cyclicargolithus floridanus, Calcidiscus premacintyrei, Discoaster variabilis,* and *Coccolithus miopelagicus.*

In Samples 160-971A-5X-CC through 10X-CC the quantity of the Pleistocene taxa diminishes greatly, as samples are dominated by middle Miocene taxa with lesser amounts of Late Cretaceous to Pliocene taxa. Clasts are abundant. Owing to a paucity of in situ Pleistocene nannofossils in this interval, the samples could not be placed into a zonation. Many of the clasts in this interval are devoid of nannofossils, whereas others are early to middle Miocene in age (Burdigalian-Langhian). Similar to Site 970, some of the clasts contain Late Cretaceous and middle Eocene age assemblages reworked into Miocene.

An intercalation of pelagic sediment that contains abundant and well-preserved nannofossils was recovered in Core 160-971A-10X. From Samples 160-971A-10X-1, 17 cm, through 10X-1, 111 cm, large *Gephyrocapsa* is present, which indicates Zone MNN19d. The presence of both *Calcidiscus macintyrei* and *G. oceanica* s.l. in Samples 160-971A-10X-3, 30 cm, through 10X-3, 133 cm, indicates that these samples are within Zone MNN19b. *G. oceanica* s.l. is absent from Sample 160-971A-10X-4, 103 cm, which together with the absence of *Discoaster brouweri* marks Zone MNN19a. The accompanying assemblage includes small *Gephyrocapsa, P. lacunosa,* and *C. macintyrei.*

Zone MNN18 was observed in Samples 160-971A-10X-5, 140 cm, through 11X-1, 117 cm, as indicated by the presence of *D. brouweri* in the absence of *Discoaster pentaradiatus* and *Discoaster surculus.* The accompanying assemblage is similar to that of previous zones, but includes *D. triradiatus.*

Samples 160-971A-11X-3, 115 cm, through 11X-CC contain nannofossils from Zone MNN17–16b. This zone is recognized as the interval between the last occurrence of *D. pentaradiatus* and the last common occurrence of *Discoaster tamalis.* The accompanying assemblage includes small *Gephyrocapsa, P. lacunosa, D. brouweri,*

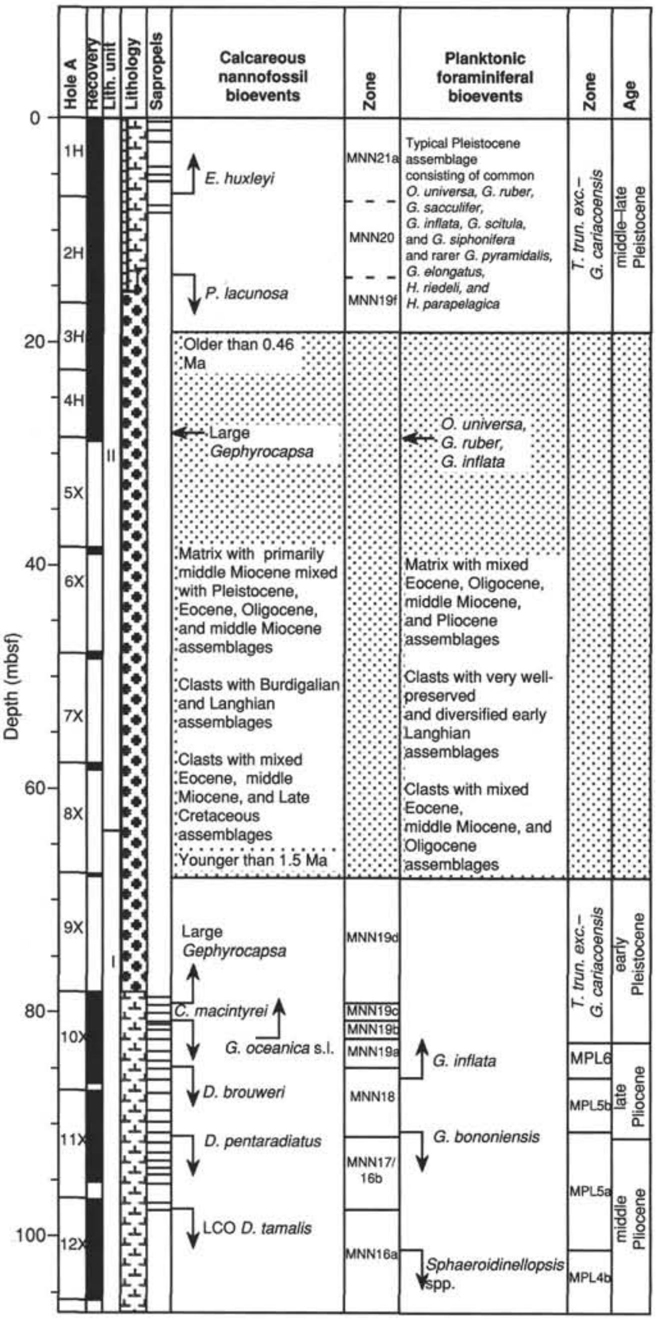

Figure 22. Composite of biostratigraphic events recognized in sediments recovered from Hole 971A including the lithostratigraphic record.

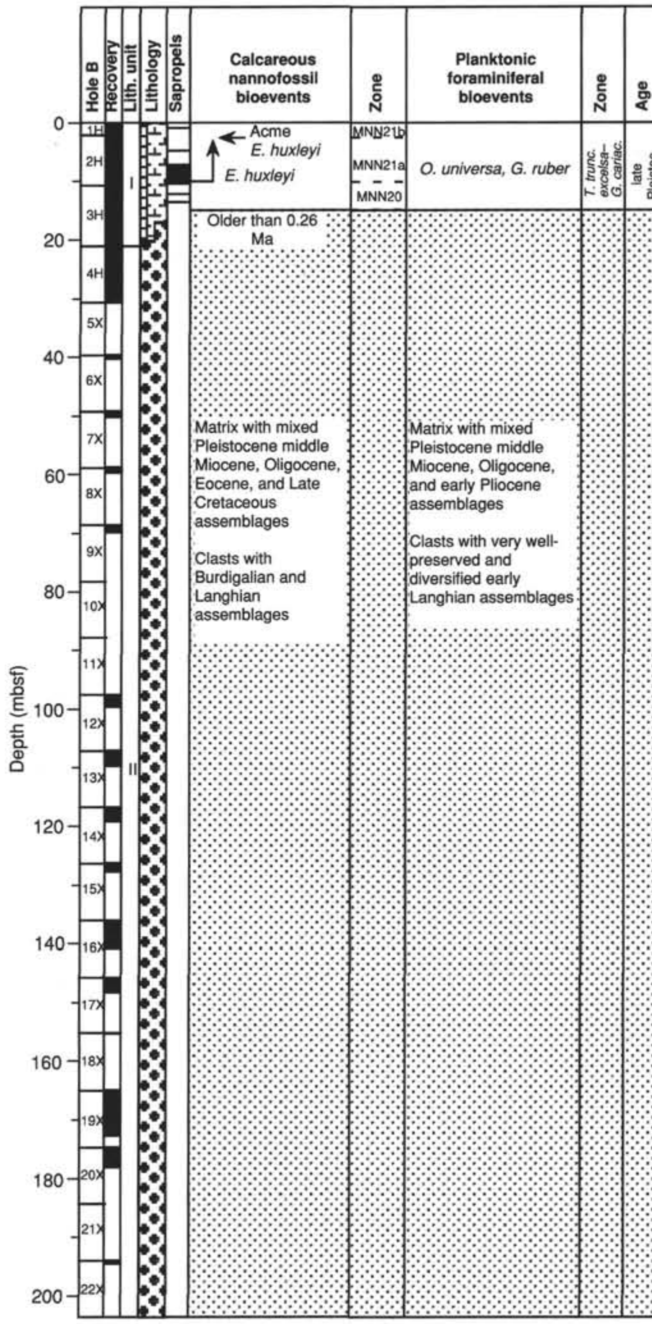

Figure 23. Composite of biostratigraphic events recognized in sediments recovered from Hole 971B including the lithostratigraphic record.

Discoaster surculus, Discoaster intercalaris, and small reticulofenestrids.

Samples 160-971A-12X-1, 65 cm, through 12X-CC contain nannofossils belonging to Zone MNN16a. This zone is identified by the common occurrence of *D. tamalis* above the last occurrence of *Reticulofenestra pseudoumbilicus.* The accompanying assemblage is similar to that found in the preceding zone.

Hole 971B

Hole 971B was drilled on the basin floor adjacent to the Napoli mud volcano. Sediment recovered from the first two cores of this site is hemipelagic ooze that contains nannofossils of late to middle Pleistocene age (Fig. 23). Locally, reworking is extensive. From Cores 160-971B-3H through 22X, rare Pleistocene taxa were observed with abundant middle Miocene nannofossils. Eocene and Oligocene species are rare to few.

The first three zones in Hole 971B are identified based on the presence and abundance of *E. huxleyi.* From the seafloor through Sample 160-971B-1H-CC, *E. huxleyi* is abundant, which represents the acme zone of this species (MNN21b). The accompanying assemblage includes *G. oceanica* s.l., *Calcidiscus leptoporus,* small *Gephyrocapsa,* and *Syracosphaera pulchra.* In the interval from Samples 160-971B-2H-1, 23 cm, through 2H-7, 70 cm, *E. huxleyi* fluctuates from common to not present; therefore, these samples were included in Zone MNN21a. Samples 160-971B-3H-1, 70 cm, and 3H-CC, contain neither *E. huxleyi* nor *P. lacunosa* and were placed into Zone

MNN20. Reworking varies in these samples from minor to common and consists primarily of middle Miocene taxa as described in Hole 971A. Specimens of *Dictyococcites bisecta, Sphenolithus heteromorphus, Sphenolithus predistentus, Sphenolithus ciperoensis,* and *C. floridanus* are common and represent middle Miocene and Paleogene material that was redeposited during the Pleistocene.

In the interval from Cores 160-971B-4H through 22X, definitive Pleistocene and Pliocene taxa are rare or absent. Although single specimens of some biomarkers were recognized above Core 160-971B-15X, the paucity of these biomarkers coupled with the fluctuation of the Pleistocene taxa throughout the section prevents zonation of the nannofossil assemblage. Knowing that most, if not all, of the sediments have been redeposited or reworked, only broad interpretations based on first appearance markers can be used confidently. Additional shore-based work involving more samples and concentration techniques may allow the zonation of some of these intervals. However, the results of shipboard studies show that Core 160-971B-14X and above are Pleistocene, based on the presence of very rare specimens of *G. oceanica* s.l. The age of sediments below Core 160-971B-14X could not be determined with confidence. The sediments within this interval contain middle Miocene taxa, as described previously.

Hole 971C

Hole 971C consists of two cores. Core 160-971C-1H contains a predominately Pleistocene assemblage, whereas a mixed assemblage containing Pleistocene, middle Miocene, and some Paleogene taxa was observed in Core 160-971C-2H. In the interval from Samples 160-971C-1H-1, 16 cm, through 1H-CC, *E. huxleyi* fluctuates from common to rare. Therefore, these samples were included in Zone MNN21a. The accompanying assemblage includes small *Gephyrocapsa, G. oceanica* s.l., *C. leptoporus,* and *S. pulchra.* Sample 160-971C-2H-CC contains few specimens of *P. lacunosa* and was tentatively placed into Zone MNN19f. Reworking varies from minor to common in those samples and consists primarily of middle Miocene taxa.

Holes 971D and 971E

Holes 971D and 971E were drilled into the crest of the Napoli mud volcano and recovered sediments of little biostratigraphic value. These holes are presumably closer than the other holes to the source of active mud extrusion. Owing to the high gas content of the cores, Holes 971D and 971E were limited to five and three cores, respectively. The sediments recovered are homogeneous gray muds that contain common nannofossils dominated by middle Miocene species. Qualitative assessment of the nannofossil assemblage from Holes 971D and 971E indicates that although the assemblage in all of the cores is predominantly middle Miocene, the approximate percentage of Eocene and Oligocene taxa is greater than in the other holes drilled into the Napoli mud volcano during Leg 160. Specifically, the Paleogene species *S. predistentus, Sphenolithus distentus, E. formosa,* and *S. ciperoensis* are more abundant than at the previous mud volcano sites. As with the lower portion of Hole 971B, in situ Pleistocene species are either very rare or absent. *E. huxleyi* is the only Pleistocene marker that was recognized from these holes. Sample 160-971D-1H-CC contains a rare Pleistocene assemblage that includes *E. huxleyi,* which classifies this sample as Zone MNN21. The remaining four cores in Hole 971D and the four cores from Hole 971E could not be definitively dated as Pleistocene.

Planktonic Foraminifers

Hole 971A

Planktonic foraminifers were analyzed in all core catchers in addition to samples from within the cores. Both matrix and clast lithologies were sampled when simultaneously observed in the mud breccia or when pelagic sediments were recovered.

The mud breccia contains reworked and poorly preserved planktonic foraminifers ranging in age from late Oligocene to Pliocene, in addition to better-preserved Pleistocene faunas (Fig. 22). Reworked specimens are rare to common, whereas Pliocene specimens are rare to abundant near the transition to pelagic sedimentation.

Upper Pleistocene pelagic sediments within the *Truncorotalia truncatulinoides excelsa–Globigerina cariacoensis* Zones were recovered in Cores 160-971A-1H and 2H. Planktonic foraminiferal assemblages consist of well-preserved and diverse faunas, including *Orbulina universa, Globigerinoides ruber, Globigerinoides elongatus, Globorotalia inflata, Globorotalia scitula, Globigerina bulloides, Globigerina falconensis, Globigerinita glutinata, Globigerinita juvenilis, Globigerinella siphonifera,* and *Turborotalita quinqueloba.* Rarer forms include *Orbulina bilobata, Globigerinoides pyramidalis, Globigerinoides gomitulus, Globigerinoides conglobatus,* and *Globigerina calida* along with very rare *Hastigerinopsis riedeli* and *Hastigerina parapelagica.*

An intercalation of the mud breccia within the pelagic sedimentary sequence was observed from Cores 160-971A-3H through 9X. The matrix is similar to that observed at the Milano Dome. It contains an abundance of reworked middle Miocene (mainly Burdigalian-Langhian) together with rare Eocene and Oligocene to Pliocene taxa. The clasts are similar to those studied at the Milano Dome. Some of them contain the typical middle Miocene assemblages assigned to *Praeorbulina glomerosa* s.l.–*Orbulina suturalis* Zones, whereas others contain mixed Eocene, Oligocene, middle Miocene, and Pliocene taxa.

Lower Pleistocene through middle Pliocene in situ sediments, spanning the interval from the lower part of *T. truncatulinoides excelsa–G. cariacoensis* interval to Zone MPL6, were found in Cores 160-971A-10X through 12X. The Pliocene planktonic foraminiferal assemblages are similar to those previously observed at Sites 964 through 969 and are generally well preserved and diverse. Sample 160-971A-10X-CC contains assemblages similar to those observed in Cores 160-971A-1H and 2H, however, no markers were observed. It was assigned to the lower Pleistocene by comparison with nannofossil data.

Samples 160-971A-10X-2, 123–125 cm, through 10X-6, 55–57 cm, contain Zone MPL6. The assemblage is similar to those observed in Cores 160-971A-1H and 2H, in addition to some Pliocene taxa (e.g., *Sphaeroidinella dehiscens* and *Globigerinoides obliquus*). In Sample 160-971A-10X-5, 147–149 cm, *S. dehiscens* occurs within the *Truncorotalia truncatulinoides excelsa* Zone.

Zone MPL5b was observed in Samples 160-971A-10X-CC through 11X-1, 96–98 cm. The top of this zone was placed with the lowest occurrence of *Globorotalia inflata* in Sample 160-971A-10X-6, 55–57 cm, and the bottom with the highest occurrence of *Globorotalia bononiensis* in Sample 160-971A-11X-3, 85–87 cm. This latter species also permits the recognition of Zone MPL5a through Sample 160-971A-12X-2, 82–84 cm.

The highest occurrence of *Sphaeroidinellopsis* spp. in Sample 160-971A-12X-3, 138–140 cm, marks the upper boundary of Zone MPL4b. This zone is identified through the bottom of the hole in Sample 160-971A-12X-6, 77–79 cm. Rare reworking of middle Miocene taxa was observed in Samples 160-971A-11X-4, 79–81 cm, and 160-971A-12X-3, 138–140 cm.

Hole 971B

Hole 971B was drilled on the floor of the moat structure adjacent to the Napoli mud volcano. Planktonic foraminifers were analyzed in all core catchers in addition to samples from within the cores. The mud with only scattered clasts that was recovered in this hole (Fig. 23) contains reworked and poorly preserved planktonic foraminifers ranging in age from late Oligocene to Pliocene, in addition to better preserved Pleistocene faunas. Reworked specimens are rare to common whereas Pleistocene specimens are rare to abundant within the pelagic sediments.

The uppermost sediments contain Pleistocene planktonic foraminiferal assemblages similar to those observed at Sites 963 through 969. They consist of common *O. universa, G. ruber, G. elongatus, G. pyramidalis, G. scitula, G. bulloides, G. falconensis, G. glutinata, G. juvenilis, T. quinqueloba,* and *Neogloboquadrina acostaensis.* Rarer are *G. siphonifera, O. bilobata,* and dextral *Neogloboquadrina pachyderma.*

The interval of mud with scattered clasts was observed from Cores 160-971B-3H through 22X. The matrix in this interval contains foraminiferal assemblages of rare to common Pliocene-Quaternary species along with common to rare taxa of Oligocene, middle Miocene (mainly Burdigalian-Langhian), and Pliocene age. The clasts are similar to those studied for the Milano Dome. Some of them contain the typical middle Miocene assemblages assigned to the *P. glomerosa* s.l.–*O. suturalis* Zones.

Holes 971C, 971D, and 971E

Only the core catchers of the 10 cores recovered at Holes 971C, 971D, and 971E were studied. They all contain the mud breccia previously observed at Hole 971A. No substantial differences were observed concerning the matrix and clasts. The matrix usually contains a Burdigalian-Langhian foraminiferal assemblage together with rarer Quaternary taxa. The clasts contain Burdigalian–early Langhian Miocene assemblages.

Diatoms

Abundant, well-preserved opal phytoplankton skeletons consisting of predominant diatoms and some silicoflagellates were observed in Samples 160-971B-2H-6, 50 cm, through 2H-CC and 160-971C-2H-1, 135 cm, through 2H-4, 15 cm. These samples were collected from a sapropel interpreted as S5 (see "Lithostratigraphy" section, this chapter). Diatom assemblages resemble those of sapropel D (= S5) of Core TR72-22 from the southern Aegean Sea (Schrader and Matherne, 1981), but are characterized by more dominant specimens of the following species: *Thalassiothrix frauenfeldii, Thalassiothrix longissima, Thalassionema bacillaris, Thalassionema nittzachioides,* spores of *Chaetoceros* spp., and *Rhizosolenia* sp. (*Rhizosolenia calcar-avis* in Schrader and Matherne, 1981). These diatoms and silicoflagellate assemblages exhibit excellent preservation, which probably resulted from rapid burial by mud and silt.

In the scenario for sapropel formation proposed by Rohling (1994), sapropels with high organic content, especially S5, contain abundant *Neogloboquadrina* and nannofossils that reflect the presence of a deep chlorophyll maximum (DCM) and increased productivity. Therefore, the presence of abundant, well-preserved diatoms in Hole 971B may be relevant to sapropel formation in the Eastern Mediterranean.

PALEOMAGNETISM

Detailed paleomagnetic studies were not attempted at Site 971 because of the chaotic nature of the sediment associated with the Napoli mud volcano. The archive halves from the overlying nannofossil clay and nannofossil ooze of lithostratigraphic Unit I (see "Lithostratigraphy" section, this chapter) from Sections 160-971B-1H-1 through 2H-5 and 160-971C-1H-1 through 2H-7 were measured on the shipboard pass-through cryogenic magnetometer after AF demagnetization at 25 mT. NRM intensities were measurable throughout and were well above the noise level of the magnetometer (Fig. 24). Peaks in magnetic intensity from Hole 971B generally correspond to peaks

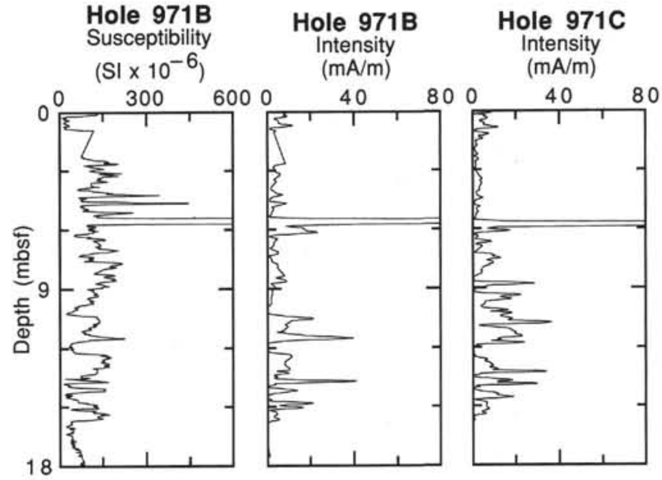

Figure 24. Magnetic susceptibility record of Hole 971B and NRM intensity after AF demagnetization at 25 mT for Holes 971B and 971C.

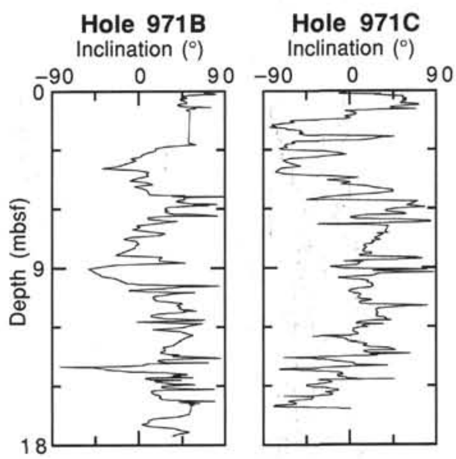

Figure 25. Paleomagnetic inclinations measured on archive-half cores using the shipboard pass-through magnetometer for Holes 971B and 971C after AF demagnetization at 25 mT.

in magnetic susceptibility (Fig. 24). A large peak in the intensity and susceptibility at approximately 5.60 mbsf in Hole 971B occurs at 5.80 mbsf in the intensity record of Hole 971C (Fig. 24) and is attributed to a thick ash layer in both holes (see "Lithostratigraphy" section, this chapter). The general correspondence between susceptibility and intensity in Hole 971B suggests strong lithologic control of the intensity at this site. The inclination records from Holes 971B and 971C are highly variable within each hole and show little similarity between holes (Fig. 25). The inclination records are therefore not considered to reflect changes in the magnetic field, but rather, probably reflect a disturbed sedimentation process that includes debris flows (see "Lithostratigraphy" section, this chapter). The paleomagnetic data shed little light on the process of mud-flow emplacement associated with the Napoli mud volcano.

INORGANIC GEOCHEMISTRY

Interstitial-water samples were obtained at Site 971 from Holes 971A through 971D, which form a transect from the rim toward the crest of the Napoli mud volcano. The standard ODP titanium/stainless-steel squeezer (Manheim and Sayles, 1974) and a plastic-lined

Table 5. Results of pore-water analysis for Site 971.

Core, section, interval (cm)	Depth (mbsf)	pH	Alkalinity (meq/L)	Salinity (g/kg)	Cl^- (mM)	Mg^{2+} (mM)	Ca^{2+} (mM)	SO_4^{2-} (mM)	NH_4^+ (μM)	SiO_2 (μM)	K^+ (mM)	Li^+ (μM)	Na^+ (mM)
160-971A-													
1H-3, 140–150	4.40	7.70	3.040	40.8	678	64.2	11.7	32.62	220	209	12.4	40.0	508
2H-5, 140–150	14.40	7.44	3.261	48.0	821	67.4	14.3	34.54	505	174	13.1	53.0	625
3H-3, 130–150	20.90	—	—	56.3	956	79.0	15.8	34.09	791	137	15.0	75.0	740
4H-3, 135–150	26.85	7.79	2.879	62.0	1169	93.6	19.1	36.86	1114	131	18.3	90.0	907
6X-1, 56–71	38.76	—	—	98.0	1648	140.4	30.1	33.49	1888	135	28.1	111.0	1318
10X-1, 135–150	78.35	6.94	1.723	158.0	2864	360.7	45.2	37.94	3248	111	71.8	112.0	2267
11X-4, 135–150	92.55	6.92	1.321	175.0	2977	423.4	47.6	36.53	3316	104	82.4	119.0	2460
12X-5, 135–150	103.65	6.86	1.086	182.0	3203	495.2	56.9	40.92	3707	90	94.3	125.0	2641
160-971B-													
1H-1, 104–109	1.04	7.56	3.681	39.8	641	—	—	34.18	145	174	12	31	—
2H-4, 140–150	8.10	7.40	6.933	47.0	810	—	—	19.70	626	244	12	43	—
3H-4, 140–150	17.60	7.57	8.544	58.3	1047	—	—	7.58	746	286	10	45	—
4H-4, 135–150	27.05	7.45	9.506	75.5	1402	—	—	0.74	1024	349	10	47	—
7X-1, 115–135	50.45	—	—	147.6	2862	—	—	1.63	2550	113	11	84	—
8X-1, 61–81	59.51	7.53	4.609	154.0	2952	—	—	5.61	2519	150	11	86	—
9X-CC, 0–10	69.75	—	—	175.0	3400	—	—	4.14	2144	90	10	90	—
12X-2, 0–20	98.88	—	—	243.0	4195	—	—	4.83	4975	78	13	67	—
13X-1, 130–150	108.40	—	—	218.0	4082	—	—	3.20	4975	109	13	68	—
14X-1, 130–150	118.00	—	—	238.0	4453	—	—	5.47	5713	84	13	71	—
15X-1, 96–116	127.26	—	—	233.0	4331	—	—	4.91	5306	65	12	75	—
16X-2, 124–144	138.74	—	—	212.0	3984	—	—	2.95	5653	78	11.10	95	—
17X-3, 0–20	148.53	—	—	206.0	3938	—	—	1.96	5246	94	11.60	108	—
19X-2, 130–150	167.70	—	—	200.0	3669	—	—	2.73	8473	100	12.50	132	—
20X-3, 0–26	177.40	—	—	185.0	3468	—	—	2.19	8292	218	12.70	414	—
160-971D-													
1H-1, 135–150	1.35	7.02	55.148	258.0	4688	—	—	12.88	581	218	5	179	—
1H-2, 135–150	2.85	7.12	82.935	282.0	5163	—	—	16.45	641	193	5	195	—
1H-4, 135–150	5.85	7.20	67.902	293.0	5408	—	—	15.34	—	183	5	200	—
2H-2, 135–150	10.85	6.99	67.808	292.0	5295	—	—	13.29	671	185	5	193	—
2H-4, 135–150	13.85	7.48	65.363	295.0	5348	—	—	14.12	708	115	5	183	—
3H-4, 135–150	23.35	7.45	73.731	297.0	5354	—	—	13.81	799	123	5	185	—
4H-4, 135–150	32.85	7.25	70.593	300.0	5365	—	—	11.72	701	152	5	183	—
5H-1, 135–150	37.85	7.33	60.723	297.0	5310	—	—	14.88	723	104	5	168	—
5H-6, 135–150	45.35	8.19	65.919	298.0	5334	—	—	12.96	799	55	5	146	—
160-971E-													
1H-1, 140–150	1.40	7.34	75.793	200.0	3535	—	—	19.06	690	255	7.7	8	—
1H-2, 140–150	2.90	7.18	83.598	238.0	4242	—	—	23.51	980	207	8.2	193	—
1H-4, 140–150	5.90	7.10	84.760	278.0	5010	—	—	28.72	1413	166	8.4	225	—
1H-6, 140–150	8.90	7.25	85.646	295.0	5260	—	—	29.59	1486	150	8.5	230	—
2H-2, 140–150	12.40	7.55	90.376	283.0	5158	—	—	28.09	1480	100	11.3	232	—
2H-5, 130–140	16.80	7.50	82.181	293.0	5281	—	—	16.12	1380	119	10.5	224	—
3H-1, 135–150	20.35	7.70	73.621	282.0	5128	—	—	26.03	1300	86	10.9	213	—
3H-7, 69–84	27.81	7.88	76.780	300.0	5325	—	—	31.58	1460	78	12.0	208	—

Note: — = no data.

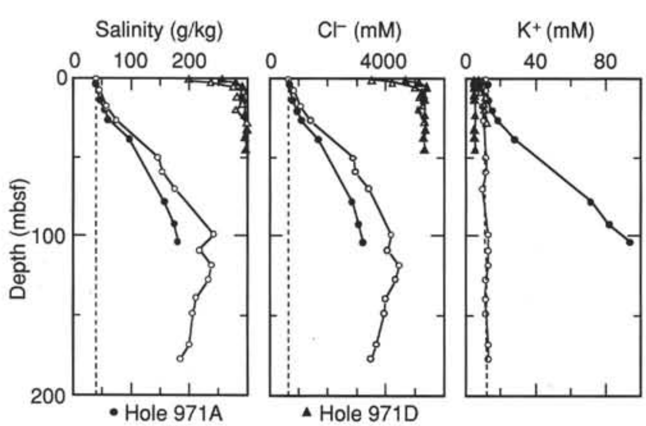

Figure 26. Pore-water vs. depth profiles at Holes 971A, 971B, 971D, and 971E for salinity, chlorinity, and potassium. The dashed line indicates the bottom-water concentration.

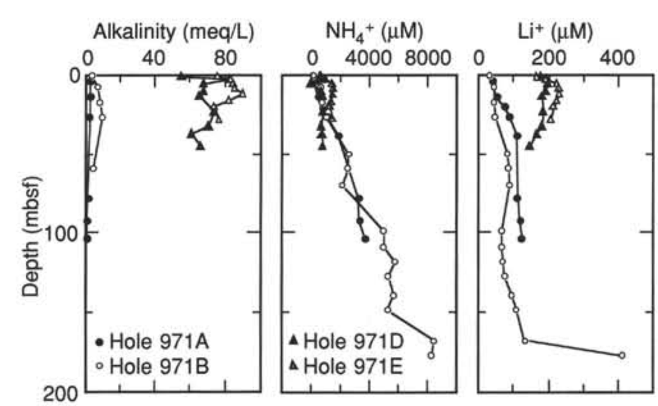

Figure 27. Pore-water vs. depth profiles at Holes 971A, 971B, 971D, and 971E for alkalinity, ammonium, and lithium.

squeezer (Brumsack et al., 1992) were used for pore-water squeezing. In total, 40 samples were retrieved, covering a depth range from 1.5 to 178 mbsf, and subsequently analyzed for salinity, alkalinity, chloride, sulfate, lithium, potassium, calcium, magnesium, ammonium, and silica using the methods described in the "Explanatory Notes" chapter (this volume). As the available data exhibit a large contrast between the two crestal holes relative to the two slope holes, we discuss the data separately. The analytical results are listed in Table 5.

Holes 971A and 971B

Holes 971A and 971B, located at the outer rim of the Napoli mud volcano, are characterized by an initially gradual increase in salinity

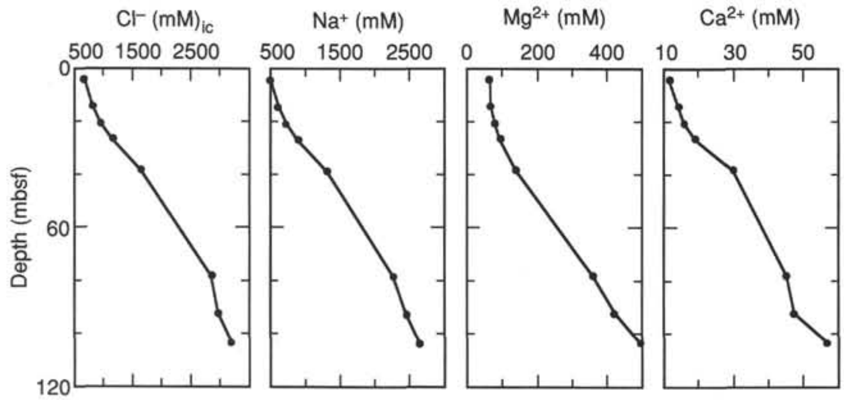

Figure 28. Pore-water vs. depth profiles at Hole 971A for chloride, sodium, magnesium, and calcium.

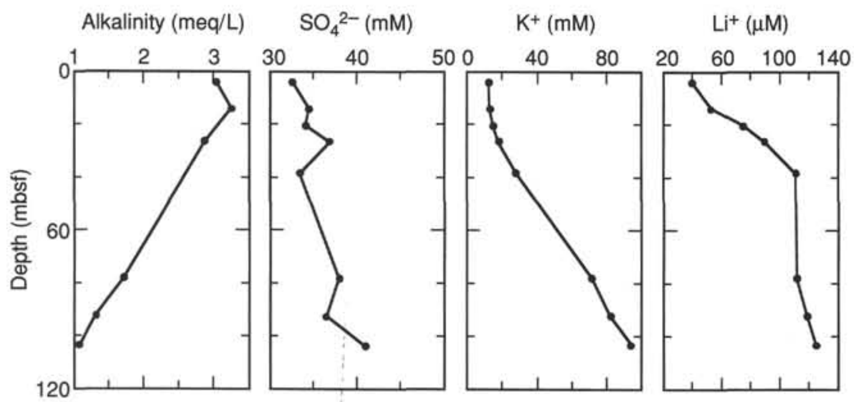

Figure 29. Pore-water vs. depth profiles at Hole 971A for alkalinity, sulfate, potassium, and lithium.

with depth for the top 30 m, followed by a sharper increase between 30 and 100 mbsf. The salinity below 100 mbsf in Hole 971A decreases slightly (Fig. 26).

Not only do the salinity and chlorinity of both holes seem to have similar concentration gradients, but also the alkalinity, potassium, and lithium profiles exhibit similar concentration vs. depth profiles for these holes. Alkalinity remains close to the seawater concentration. In view of the relatively moderate ammonium concentrations, only minor carbonate diagenesis may have occurred at these two holes (Fig. 27).

The increase in salinity in Hole 971A corresponds to an increase in the concentrations of chloride, sodium, magnesium, calcium, potassium, and lithium (Figs. 28, 29). The concentration of sulfate demonstrates a minor increase vs. depth. The moderate ammonium concentrations suggest that only minor bacterially mediated degradation of organic matter through sulfate-reducing processes has occurred. The slight decrease in alkalinity indicates some carbonate precipitation, although this is not reflected in the calcium profile. As stated previously, the calcium profile is dominated by a major upward salinity flux, thereby masking other possible processes.

The potassium vs. depth profile is distinctly different between Holes 971A and 971B; in Hole 971B, the potassium remains almost constant, whereas in Hole 971A a sharp increase occurs below a depth of approximately 20 mbsf (Fig. 26). At this time, we do not have a satisfactory explanation for this difference. In addition, a large increase occurs in the lower part of the lithium vs. depth profile for Hole 971A. Further study is needed to exclude possible sample contamination for this sample and to search for the origin of this extreme increase.

Holes 971D and 971E

Holes 971D and 971E were drilled on the crestal part of the Napoli mud dome and are characterized by extremely high salinity, alkalinity, and lithium values near the sediment/seawater interface (Fig. 26). In contrast, the concentration of potassium remains close to seawater values. The salinity profile is identical in shape to the chlorinity profile.

Similar steep concentration vs. depth profiles for the Napoli Dome sediments were observed by Van Santvoort and de Lange (in press). In view of the low ammonium concentrations observed in these holes, the high alkalinity values in the crest sediments cannot be explained by sulfate reduction alone. It seems, therefore, that methane oxidation occurs up to relatively shallow depth levels in these sediments, thereby producing carbonate (i.e., alkalinity). The mousselike texture of the sediments, as well as the headspace analyses, indicates that methane occurs at relatively shallow depths at these sites (see "Lithostratigraphy" and "Organic Geochemistry" sections, this chapter).

The relatively high lithium concentrations in the crest sediments are most likely related to the high ammonium concentrations, inducing exchange reactions with mineral surfaces in a manner similar to those reported for the other Leg 160 sites.

ORGANIC GEOCHEMISTRY

Volatile Hydrocarbons

As part of the shipboard safety and pollution-prevention monitoring program, hydrocarbon gases were analyzed in each core of Holes 971A, 971B, 971D, and 971E by the headspace technique and, where gas pockets occurred, also in vacutainer gas samples. Only minor concentrations of methane in the range of 6 to 52 ppm were recorded in Hole 971A. In contrast to this, gas was highly abundant in Holes 971B, 971D, and 971E (Table 6) as visually obvious from core expansion resulting from abundant gas pockets and the explosion of the core liner of Core 160-971E-3H.

Table 6. Hydrocarbon gas data for Site 971, headspace method and Natural Gas Analyzer.

Core, section, interval (cm)	Depth (mbsf)	C_1 (ppm)	C_2 (ppm)	C_3 (ppm)	i-C_4 (ppm)	n-C_4 (ppm)	i-C_5 (ppm)	n-C_5 (ppm)	i-C_6 (ppm)	n-C_6 (ppm)	C_1/C_2	Method
160-971B-												
1H-1, 99–104*	0.99	5										H
2H-5, 0–5*	8.20	5										H
3H-5, 0–5*	17.70	5										H
4H-5, 0–5*	27.20	1,390	35								40	H
6X-1, 0–5*	39.70	2,406	215								11	H
7X-1, 0–5*	49.30	2,580	296								9	H
8X-1, 56–61	59.46	3,082	411	6	183	2	115		6		7	H
9X-CC, 56–61	70.31	3,361	459	8	175		91		5		7	H
12X-2, 15–20	99.03	2,270	377	29	137	29	69	2	6		6	H
13X-2, 0–5	108.60	4,727	810	51	183	28	85	4	8		6	H
14X-2, 0–5	118.20	3,390	329		3	5	4		4		10	H
15X-1, 0–5	126.30	2,134	231	10	10	6	19		4		9	H
16X-1, 50–51	136.50	759,250	61,467	10,833	2335	1843	528	183	25	27	12	V
16X-3, 0–5	138.94	4,518	772	243	69	67	22	96	2		6	H
17X-2, 0–5	147.10	5,043	718	198	64	63	47	14	5	6	7	H
17X-2, 0–5	147.60	434,410	37,942	6,265	1349	877	391	75	17	13	11	V
19X-2, 0–5	166.90	677,982	69,811	9,894	2168	1195	631	144	25	25	10	V
19X-3, 0–5	167.90	15,963	2,388	533	150	100	57	13	12		7	H
20X-1, 50–51	175.00	850,772	85,142	11,278	2093	1616	588	162	25	24	10	V
20X-2, 0–5	175.90	20,126	2,764	563	164	163	87	27	4	5	7	H
160-971D-												
1H-3, 0–5	3.00	4,549	234	10	64	7	71	3	72		19	H
1H-4, 129–134	5.79	4,577	178	9	60	5	55	2	4	1	26	H
1H-5, 50–51	7.23	714,190	15,856	333	1209	61	559	16	37	7	45	V
2H-3, 0–5	11.00	2,599	124	6	35	5	25	1	4		21	H
2H-4, 50–51	13.00	714,802	16,560	353	1177	57	400	12	27	6	43	V
2H-5, 0–5	14.00	6,353	194	9	47	5	34	2	4	1	33	H
3H-5, 0–5	23.50	13,037	737	26	153	9	83	3	5	2	18	H
3H-5, 50–51	24.00	898,344	20,528	467	1565	71	483	14	31	7	44	V
4H-5, 0–5	33.00	6,210	379	22	118	7	57	2	3	1	16	H
4H-5, 50–51	33.50	690,855	15,821	341	1205	45	336	7	18	4	44	V
5H-3, 50–51	40.00	863,998	21,240	517	1488	72	418	9	24	4	41	V
5H-7, 0–5	45.50	5,764	410	37	118	10	61	2	4	1	14	H
5H-7, 100–102†	46.50	8,783	828	201	28	37	10	8	2	2	11	H
160-971E-												
1H-2, 50–51	2.00	630,946	20,029	130	765	17	270	8	21	6	32	V
1H-3, 0–5	3.00	4,233	287	5	55	3	69	3	11	5	15	H
2H-3, 0–5	12.50	6,525	632	12	117	5	74	3	6	2	10	H
2H-3, 50–51	13.00	901,557	40,450	283	1868	48	616	18	53	15	22	V
3H-3, 50–51	21.00	782,397	32,666	199	1506	36	480	14	34	10	24	V

Notes: * = samples analyzed with GC for gaseous hydrocarbons up to propane only; all other samples analyzed with Natural Gas Analyzer up to hexane; † = halite sample dissolved in water; H = headspace; V = vacutainer.

Methane concentrations from headspace analysis were up to about 20,000 ppm in Hole 971B, up to about 13,000 ppm in Hole 971D, and up to about 6500 ppm in Hole 971E. Significant concentrations of higher hydrocarbons (straight-chain and 2-methyl compounds from ethane to n-hexane were identified, but a variety of additional unidentified compounds were present as well) were also found in almost all samples. Among them, branched compounds predominate over the straight carbon-chain isomers.

Vacutainer samples from all holes contained very high methane concentrations, varying from 434,000 to 902,000 ppm. Similarly, ethane and higher hydrocarbons were more abundant (Table 6). Generally, the downhole profiles of methane do not show significant variations (Fig. 30). This, in accordance with the salinity values (see "Inorganic Geochemistry" section, this chapter), indicates that gas hydrates are absent (or of minor importance) and is considered as evidence of a continuous gas flow to the sediment surface. Differences in methane/ethane ratios, which vary from about 10 to 40 between the three holes (Fig. 30) may indicate variations in the mixing of hydrocarbons of different sources (i.e., biogenic methane and higher hydrocarbons formed diagenetically by low-temperature alteration of sedimentary organic matter) in different parts of the mud volcano.

Molecular distributions of hydrocarbons with four and more carbon atoms are more consistent with diagenetic formation than with thermal generation at higher temperatures at greater depth, although a contribution of some thermogenic gas in a more complex, multiple-source mixing pattern cannot be fully excluded. The predominance of 2-methylpropane (iso-butane) and its higher homologs over the n-al-

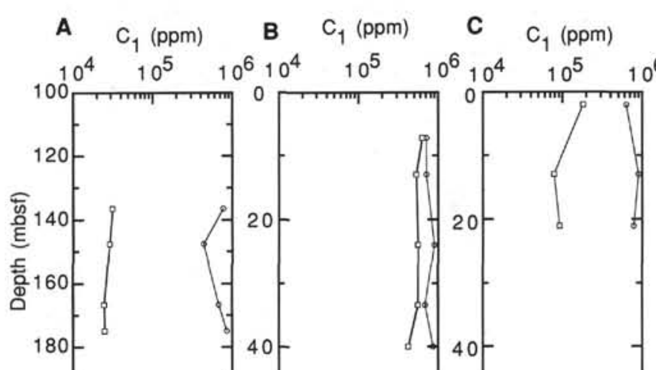

Figure 30. Downhole variation of methane concentrations (circles) and methane/ethane (C_1/C_2) ratios (squares) for vacutainer samples from (**A**) Hole 971B, (**B**) Hole 971D, and (**C**) Hole 971E.

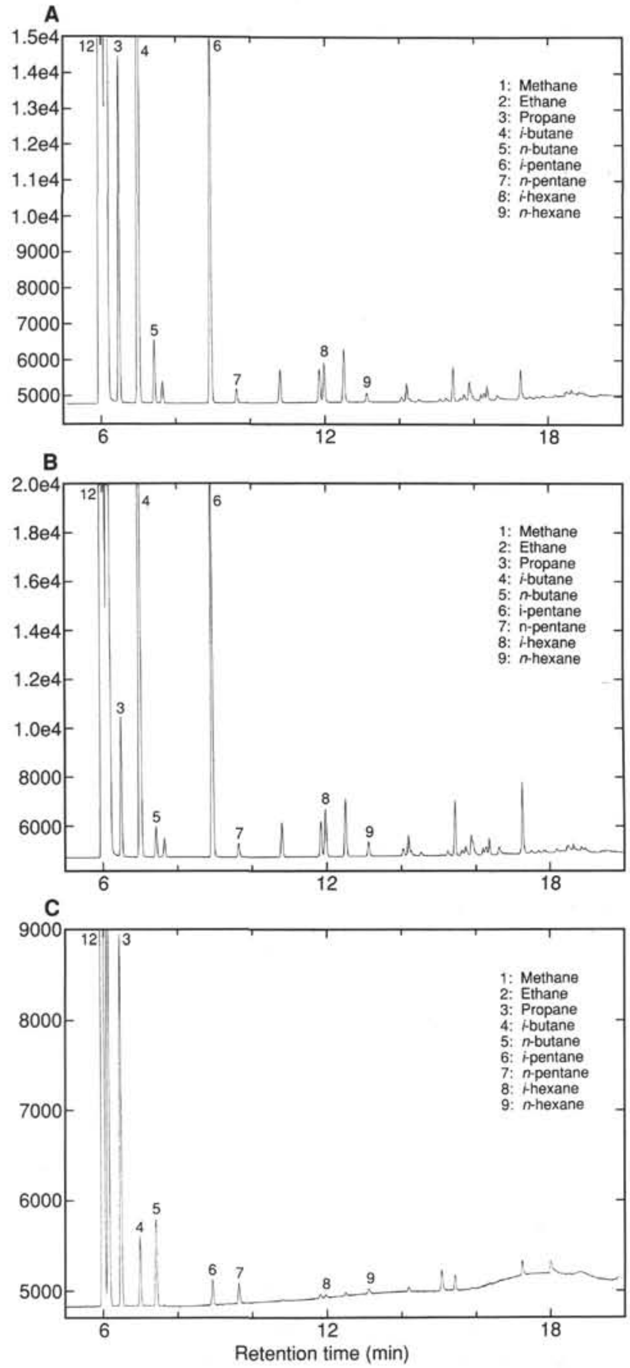

Figure 31. Gas chromatograms of light hydrocarbons, determined by the Natural Gas Analyzer, for (**A**) vacutainer sample from Section 160-971D-3H-5, (**B**) vacutainer sample from Section 160-971E-2H-3, and (**C**) headspace gas after dissolution of a piece of halite from Section 160-971D-5H-7 in water.

kane isomers with the same carbon numbers (Fig. 31A, B) are strong evidence for a low-temperature formation. A dominance of *iso-* over *n*-alkanes in deep-sea sediments was observed before by carrier-gas stripping analysis of a lower Miocene sediment (237.2 mbsf) from DSDP Site 545 on the Mazagan Escarpment (Shipboard Scientific Party, 1984) and less pronounced in Miocene/Pliocene sediments from the Walvis Ridge (100–250 mbsf at DSDP Site 532; Schaefer and Leythaeuser, 1984) and Cenomanian sediments at more than 300 mbsf on the northwest African continental margin (Shipboard Scientific Party, 1984). Only in the deeply buried Cretaceous sediments of the Angola Basin (750 to almost 1100 mbsf) do the straight-chain compounds start to become slightly more abundant than their branched counterparts (Schaefer and Leythaeuser, 1984).

Headspace analysis of a halite sample dissolved in water revealed a distribution pattern in which the *n*-alkanes are more enriched than in the vacutainer and sediment headspace samples (Fig. 31C). There are two possible explanations for this difference. Either halite clasts brought up from greater depth have retained a gas composition that was different from that presently flowing through the surface layer of the mud volcano or the halite acted as a molecular sieve and caused molecular fractionation of the gas during crystallization either at greater depth or at the depth from which it was recovered.

Carbonate and Organic Carbon

The abundances of total, inorganic, and organic carbon and of calcium carbonate in sediments from Holes 971A through 971E are summarized in Table 7. Random sampling was performed for carbonate analysis. For organic matter assessment, samples were specifically taken from dark layers that indicate enrichment in organic matter.

Carbonate contents in the pelagic sequences of Holes 971A and 971B mostly vary between 20% and 68% except for the sapropels in Cores 160-971A-10X through 12X which, with few exceptions, contain less than 20% carbonate. Mud-flow sequences in Holes 971B, 971D, and 971E typically contain about 20%–24% carbonate, whereas in Hole 971A the carbonate contents are variable (4%–39%) (Table 7).

Organic carbon was determined mainly for sediments visually distinguished by their dark colors. Sapropels in the pelagic sequences in Holes 971A and 971B contain more than 2% organic carbon and reach values as high as 16%–24% in the Pliocene (Cores 160-971A-10X through 12X). Typical organic carbon contents of mud-flow sediments are close to 0.5% (Table 7, Fig. 32).

Organic Matter Type: C_{org}/N Ratios

C_{org}/N ratios in sapropels vary from 11.5 to 22.3 (Table 7). As already observed at previous sites (see, e.g., "Organic Geochemistry" section, "Site 964," "Site 966," and "Site 967" chapters, this volume), the surprisingly high values of the C_{org}/N ratio in many of the sapropels suggest a predominance of terrestrial organic matter. Rather than following accepted lines of interpretation (e.g., Emerson and Hedges, 1988), the high C_{org}/N ratios in the sapropels are tentatively interpreted as representing an effective removal of nitrogen compounds from the marine organic matter during diagenesis; however, it cannot be ruled out that the primary marine organic matter was already poor in nitrogen-bearing constituents. C_{org}/N ratios of mud-flow sediments with organic carbon contents below 0.8% are mostly below 10, which suggests that inorganic nitrogen contributed to the measured nitrogen values.

Sulfur

Sulfur contents are reported in Table 7. With few exceptions they are higher than 2% in sapropels, with a maximum of 14.3% in Sample 160-971A-11X-5, 31–32 cm. Most of the sulfur is present as pyrite because pyrite concretions were visually detected in the sapropels and abundant disseminated pyrite was observed under the microscope. For most sapropels there is a tendency of covariation of sulfur and organic carbon contents.

PHYSICAL PROPERTIES

Physical and index properties (see "Explanatory Notes" chapter, this volume) were measured in all cores recovered from Holes 971A,

Table 7. Concentration of inorganic, total, organic carbon, calcium carbonate, total nitrogen, and sulfur for sediments from Site 971.

Core, section, interval (cm)	Depth (mbsf)	Total carbon (%)	Inorganic carbon (%)	Organic carbon (%)	$CaCO_3$ (%)	Nitrogen (%)	Sulfur (%)	C_{org}/N	C_{org}/S
160-971A-									
1H-4, 94–96	5.44	6.67	4.33	2.34	36.1	0.15	0.77	15.6	3.0
1H-4, 98–100	5.48	9.43	5.45	3.98	45.4	0.24	1.93	16.6	2.1
1H-4, 102–104	5.52	12.84	5.83	7.01	48.6	0.42	2.63	16.7	2.7
1H-4, 106–108	5.56	11.46	6.27	5.19	52.2	0.32	2.50	16.2	2.1
2H-2, 75–76	9.25		3.95		32.9				
2H-6, 75–76	15.25		5.52		46.0				
2H-6, 110–111	15.60	5.38	4.45	0.93	37.1	0.09	1.21	10.8	0.8
3H-1, 55–56	17.05	2.74	2.51	0.23	20.9	0.05	1.48		
3H-4, 55–56	21.55	2.61	2.50	0.11	20.8	0.05	1.07		
4H-1, 63–64	23.13		1.78		14.8				
4H-3, 62–63	26.12	1.48	0.43	1.05	3.6	0.06	1.44	19.1	0.7
6X-CC, 7–8	38.98	5.02	4.64	0.38	38.7	0.05	0.12	7.9	3.1
8X-1, 15–16	57.75	2.32	1.83	0.49	15.2	0.05	0.98	9.1	0.5
10X-1, 40–41	77.40		7.42		61.8				
10X-1, 98–99	77.98	16.42	0.41	16.01	3.4	0.84	9.70	19.0	1.7
10X-2, 90–91	79.40	14.28	3.77	10.51	31.4	0.55	6.44	19.2	1.6
10X-3, 16–17	80.16	14.14	3.56	10.58	29.7	0.56	7.24	19.1	1.5
10X-3, 80–81	80.80		8.17		68.1				
10X-3, 143–144	81.43	13.12	4.20	8.92	35.0	0.46	10.72	19.3	0.8
10X-4, 14–15	81.64	21.73	2.18	19.55	18.2	0.88	6.38	22.3	3.1
10X-4, 80–81	82.30		7.17		59.7				
10X-4, 120–121	82.70	23.27	0.82	22.45	6.8	1.01	9.19	22.2	2.4
10X-5, 20–21	83.20	15.24	2.63	12.61	21.9	0.61	7.03	20.8	1.8
10X-6, 15–16	84.65		7.32		61.0				
11X-1, 120–121	87.90		8.08		67.3				
11X-2, 117–118	89.37	9.02	5.80	3.22	48.3	0.21	2.56	15.2	1.3
11X-3, 13–14	89.83	11.51	6.43	5.08	53.6	0.34	5.84	14.8	0.9
11X-3, 101–102	90.71	12.33	4.78	7.55	39.8	0.41	7.59	18.2	1.0
11X-4, 60–61	91.80		7.00		58.3				
11X-5, 31–32	93.01	22.98	0.99	21.99	8.2	1.05	14.30	20.9	1.5
11X-5, 93–94	93.63	16.19	4.43	11.76	36.9	0.60	2.02	19.7	5.8
11X-6, 32–33	94.52	12.19	5.09	7.10	42.4	0.39	5.18	18.0	1.4
12X-1, 31–32	96.61	24.44	0.37	24.07	3.1	1.10	8.06	21.8	3.0
12X-2, 46–47	98.26	15.62	0.25	15.37	2.1	0.80	10.45	19.2	1.5
12X-3, 70–71	100.00		7.04		58.6				
12X-4, 50–51	101.30		6.94		57.8				
160-971B-									
1H-1, 40–41	0.40	9.37	6.38	2.99	53.1	0.26	1.75	11.5	1.7
1H-1, 86–87	0.86		6.42		53.5				
2H-1, 70–71	2.90		4.67		38.9				
2H-3, 40–41	5.60	0.60	0.60	0.00	5.0	0.02	0.00		
2H-3, 97–98	6.17	7.13	5.04	2.09	42.0	0.16	2.63	13.1	0.8
2H-5, 61–62	8.81		3.88		32.3				
2H-6, 110–111	10.80	7.73	1.81	5.92	15.1	0.37	1.92	16.0	3.1
2H-7, 18–19	11.38	8.09	3.67	4.42	30.6	0.32	1.95	13.8	2.3
3H-2, 38–39	13.58	10.64	6.49	4.15	54.1	0.33	6.18	12.6	0.7
3H-2, 110–111	14.30		4.84		40.3				
3H-3, 80–81	15.50		6.98		58.1				
3H-5, 80–81	18.50	3.12	2.80	0.32	23.3	0.06	2.82		
4H-2, 50–51	23.20		3.14		26.2				
4H-4, 90–91	26.60	3.40	3.13	0.27	26.1	0.06	2.63		
4H-5, 104–105	28.24	3.19	2.84	0.35	23.7	0.06	2.60		
6X-1, 29–30	39.99	3.22	2.87	0.35	23.9	0.06	0.44		
8X-1, 30–31	59.20	3.18	2.80	0.38	23.3	0.07	1.20		
9X-1, 30–31	68.90	2.78	2.16	0.62	18.0	0.06	0.84	10.3	0.7
13X-1, 60–61	107.70	3.07	2.61	0.46	21.7	0.06	0.55		
14X-2, 60–79	118.80		2.79		23.2				
15X-1, 70–71	127.00	2.92	2.55	0.37	21.2	0.06	0.81		
16X-1, 70–71	136.70	0.77	0.44	0.33	3.7	0.08	1.32		
16X-2, 49–50	137.99		1.53		12.7				
16X-3, 43–44	139.37	1.71	1.34	0.37	11.2	0.07	0.15		
17X-1, 84–85	146.44		1.20		10.0				
17X-2, 83–84	147.93	2.42	2.06	0.36	17.2	0.07	0.88		
19X-1, 36–37	165.26		2.34		19.5				
19X-3, 36–37	168.26	2.47	1.86	0.61	15.5	0.07	0.47	8.7	1.3
19X-4, 36–37	169.45		2.11		17.6				
19X-CC, 26–27	172.13	2.49	2.06	0.43	17.2	0.07	0.55	6.1	0.8
20X-1, 60–61	175.10		2.32		19.3				
20X-2, 60–61	176.50	2.92	2.47	0.45	20.6	0.07	0.56	6.4	0.8
160-971D-									
1H-2, 40–41	1.90		3.38		28.2				
1H-5, 39–40	6.39	3.47	3.06	0.41	25.5	0.05	1.66	8.2	0.2
2H-2, 39–40	9.89		2.98		24.8				
2H-5, 39–40	14.39		2.86		23.8				
3H-2, 39–40	19.39		2.93		24.4				
3H-5, 40–41	23.90	3.24	2.73	0.51	22.7	0.06	1.78	8.5	0.3
4H-2, 39–40	28.89		2.84		23.7				
4H-4, 39–40	31.89	3.35	2.92	0.43	24.3	0.06	1.29	7.2	0.3
5H-2, 40–41	38.40		2.90		24.2				
5H-5, 40–41	42.90	3.25	2.82	0.43	23.5	0.06	1.15	7.2	0.4
160-971E-									
1H-1, 129–130	1.29	2.60	2.22	0.38	18.5	0.07	2.69	5.4	0.1
1H-2, 39–40	1.89	3.99	3.49	0.50	29.1	0.06	2.35	8.3	0.2
1H-5, 39–40	6.39		2.46		20.5				
2H-2, 39–40	11.39	3.30	2.87	0.43	23.9	0.06	1.72	7.2	0.3
2H-4, 39–40	14.39		2.94		24.5				
3H-2, 39–40	20.89	3.67	3.19	0.48	26.6	0.05	1.37	9.6	0.4
3H-7, 39–40	27.51		3.01		25.1				

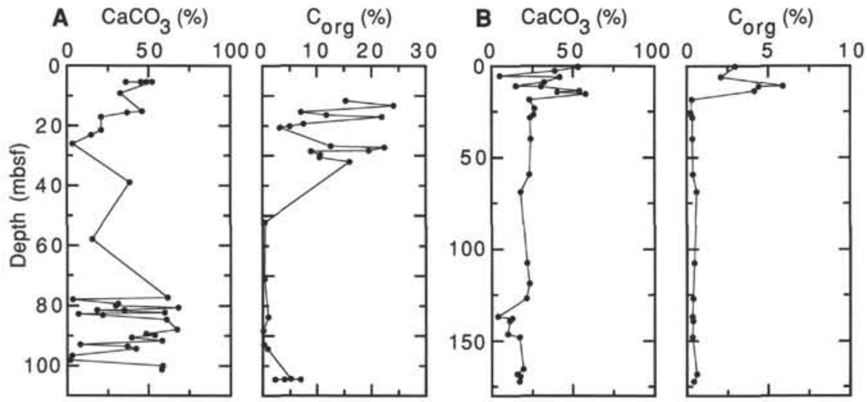

Figure 32. Downhole distribution of calcium carbonate and organic carbon concentrations in sediments from (**A**) Hole 971A and (**B**) Hole 971B.

Table 8. Index properties measured in cores from Site 971.

Core, section, interval (cm)	Depth (mbsf)	Water content (wt%)	Porosity (vol%)	Bulk density (g/cm^3) Method B	Bulk density (g/cm^3) Method C	Grain density (g/cm^3) Method B	Grain density (g/cm^3) Method C	Dry density (g/cm^3) Method B	Dry density (g/cm^3) Method C
160-971A-									
1H-1, 52–54	0.52	40.36	67.08	1.70	1.63	3.08	2.71	1.02	0.97
1H-2, 52–54	2.02	41.15	66.38	1.65	1.63	2.89	2.76	0.97	0.96
1H-3, 72–74	3.72	35.85	60.66	1.73	1.71	2.83	2.72	1.11	1.09
1H-4, 64–66	5.14	39.42	63.50	1.65	1.67	2.74	2.81	1.00	1.01
1H-5, 56–58	6.56	39.60	65.80	1.70	1.65	3.01	2.73	1.03	0.99
2H-1, 50–52	7.50	35.49	60.64	1.75	1.71	2.87	2.71	1.13	1.10
2H-2, 50–52	9.00	47.77	83.69	1.79	1.45	5.74	2.32	0.94	0.75
2H-3, 50–52	10.50	35.09	60.83	1.78	1.74	2.94	2.78	1.15	1.13
2H-4, 50–52	12.00	41.38	67.58	1.67	1.61	3.03	2.71	0.98	0.94
2H-5, 50–52	13.50	34.63	60.85	1.80	1.74	3.01	2.76	1.18	1.14

Only part of this table is reproduced here. The entire table appears on the CD-ROM (back pocket).

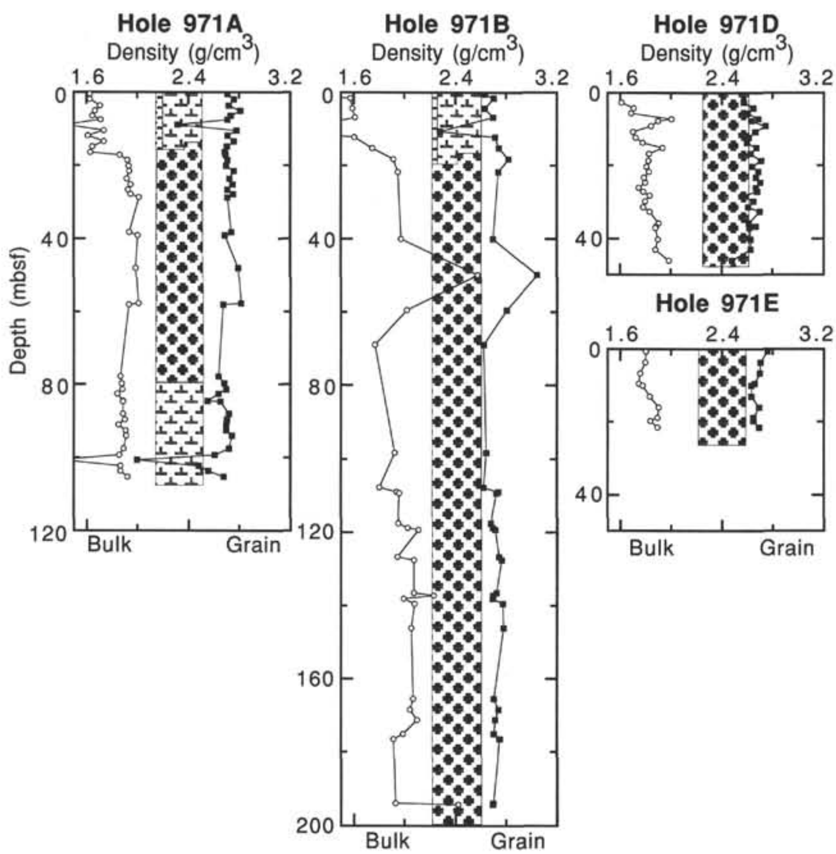

Figure 33. Index properties bulk and grain density measured in cores from Site 971, shown with lithologic summaries (see "Lithostratigraphy" section, this chapter).

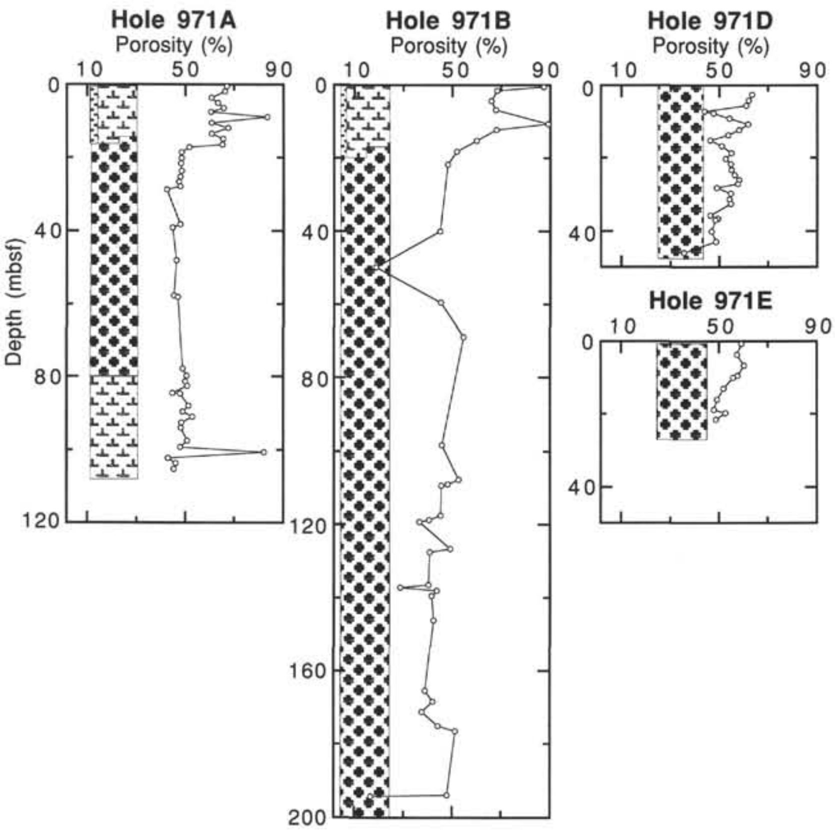

Figure 34. Index properties porosity measured in cores from Site 971, shown with lithologic summaries.

971B, 971D, and 971E. No physical properties measurements were taken in cores from Hole 971C.

Index Properties

Index properties measurements are contained in Table 8 and shown in Figures 33 and 34. To a first approximation, the index properties appear to be lithologically controlled (see "Lithostratigraphy" section, this chapter, for detailed descriptions of the lithologies referred to below). The uppermost part of Holes 971A and 971B (0–16.5 and 0–20 mbsf, respectively) contains nannofossil ooze, and this lithology corresponds to an interval of increasing bulk density, decreasing porosity, and approximately constant grain density (Figs. 33, 34), which is consistent with the effects of compaction. Nannofossil ooze was also found in Hole 971A between 71 and 106 mbsf, and index properties measurements are fairly constant through this interval.

Although the lithology in cores from Holes 971D and 971E is described as vesicle-rich, mousselike silty clay to sandy silt, the index properties trends are different in these two holes. In Hole 971D, porosity decreases and bulk density increases overall with depth. On a finer scale, bulk density increases and porosity decreases in the uppermost 8 m of Hole 971D; below that, bulk density decreases and porosity increases between 8 and 11 mbsf (Figs. 33, 34). These trends may reflect the presence of a gas-rich layer between 8 and 11 mbsf. In Hole 971E, bulk density shows a slight decrease between 0 and 10 mbsf.

Grain density in Holes 971D and 971E averages 2.64 and 2.67 g/cm^3, respectively. The physical properties of Sections 2 through 6 of Core 160-971E-3H were unmeasurable owing to a rather spectacular explosive decompression of the core. Attempts to measure the in situ density of the mousselike muddy texture proved unsuccessful. However, we infer that the exploded sections of core showed an exceptionally rapid porosity increase and density decrease, although we do not propose repetition of the experiment to test this hypothesis.

Deposits described as mud debris flows form the lithology of Hole 971A between 16.5 and 71 mbsf and of Hole 971B between 20 and 203.5 mbsf. Poor core recovery in this interval precludes definitive statements about the relationship of index properties to lithology. However, the interval from 17 to 29 mbsf in Hole 971A is well sampled, and the index properties density and porosity values are constant. Scatter in the index properties density and porosity measurements in the remainder of the debris-flow lithology of Holes 971A and 971B probably reflects the overall heterogeneous nature of this lithostratigraphic unit. In particular, variations in clast content, lithology, and size are likely first-order controls on the index properties.

Discrete-sample *P*-wave and Shear Strength Measurements

Horizontal and vertical *P*-wave velocities measured with the digital sonic velocimeter show a generally increasing trend with depth in Hole 971A (Table 9, Fig. 35). Owing to an increase in sediment cohesiveness, the measurement method was switched from DSV 1 to DSV 3 at 22.8 mbsf. Because of the presence of voids and heterogeneous matrix in the mud volcano sediments, the DSV and vane-shear measurements were difficult to obtain. Vane-shear data are presented in Table 10 and Figure 36.

GRAPE Density

MST measurements were made in some cores from Holes 971A, 971B, 971D, and 971E; however, the core recovery and presence of

Table 9. Compressional wave velocity measured in split cores from Holes 971A and 971B.

Core, section, interval (cm)	Depth (mbsf)	Measurement type	Velocity (km/s)
160-971A-			
1H-1, 50.6	0.51	DSV 1	1.57
1H-2, 50.8	2.01	DSV 1	1.53
1H-3, 65.6	3.66	DSV 1	1.55
1H-4, 56.6	5.07	DSV 1	1.57
1H-5, 50.8	6.51	DSV 1	1.60
1H-5, 50.9	6.51	DSV 1	1.60
2H-1, 50.9	7.51	DSV 1	1.57
2H-2, 49.9	9.00	DSV 1	1.55
2H-3, 49.9	10.50	DSV 1	1.54
2H-4, 50.3	12.00	DSV 1	1.56

Note: Direct DSV measurements.

Only part of this table is reproduced here. The entire table appears on the CD-ROM (back pocket).

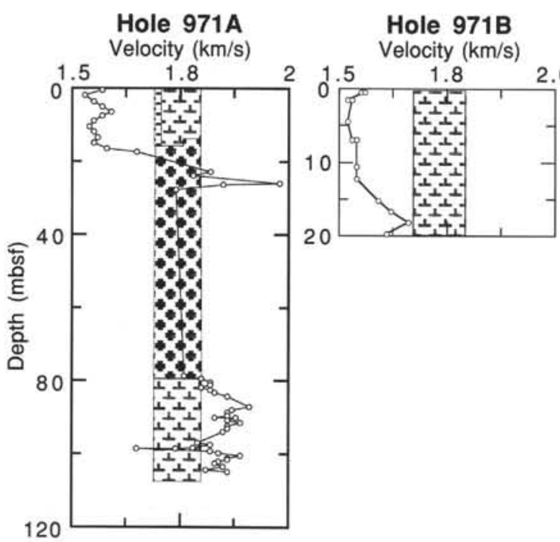

Figure 35. *P*-wave velocity measured with the DSV in cores from Site 971, shown with lithologic summaries.

Table 10. Vane shear strength measured in split cores from Hole 971A.

Core, section, interval (cm)	Depth (mbsf)	Strength (kPa)
160-971A-		
1H-1, 39.00	0.39	5.60
1H-2, 49.60	2.00	6.20
1H-3, 65.00	3.65	6.20
1H-4, 55.70	5.06	8.50
1H-5, 49.40	6.49	8.50
2H-1, 50.40	7.50	9.90
2H-2, 49.10	8.99	11.10
2H-3, 48.30	10.48	15.00
2H-4, 49.20	11.99	17.10
2H-5, 49.00	13.49	21.70

Only part of this table is reproduced here. The entire table appears on the CD-ROM (backpocket).

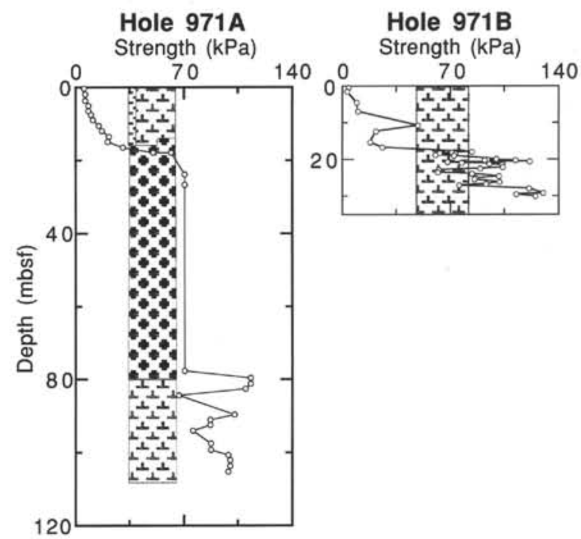

Figure 36. Vane shear strength measured in cores from Site 971, shown with lithologic summaries.

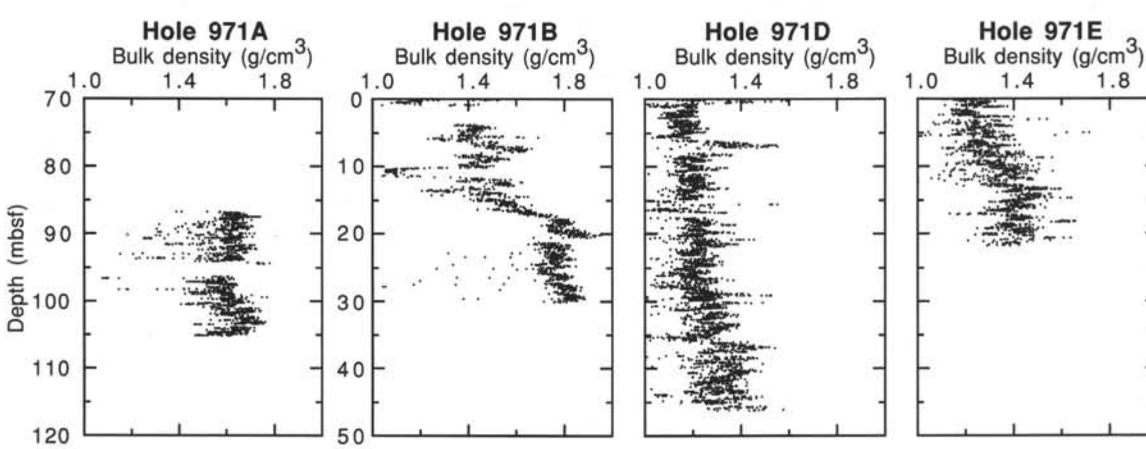

Figure 37. GRAPE densities measured in cores from Site 971 using the MST. Note the different depth range for Hole 971A.

Table 11. Thermal conductivity measured in APC cores from Hole 971A.

Core, section, interval (cm)	Depth (mbsf)	Thermal conductivity (W/[m · K])
160-971A-		
1H-1, 50	0.50	1.249
1H-2, 50	2.00	1.165
1H-3, 50	3.50	0.922
1H-4, 50	5.00	0.882
1H-5, 50	6.50	1.729
2H-1, 50	7.50	1.293
2H-2, 50	9.00	1.285
2H-3, 50	10.50	1.268
2H-4, 50	12.00	1.121
2H-5, 50	13.50	1.174

Only part of this table is reproduced here. The entire table appears on the CD-ROM (back pocket).

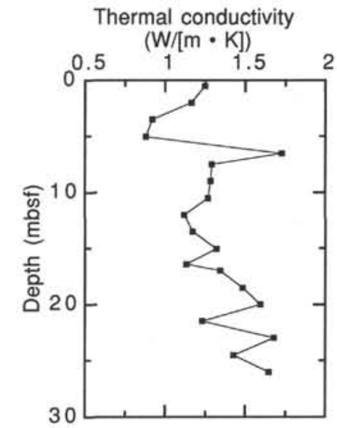

Figure 38. Thermal conductivity measured in cores from Hole 971A.

numerous gas voids and gaps limited the feasibility of taking MST measurements. Owing to these problems, the only MST data that appear reliable for Site 971 are those from the GRAPE, and these are available for at most the upper 45 m of each hole. The GRAPE densities presented in Figure 37 show a general increase of density with depth. In Hole 971B, the increase is stepwise rather than continuous, in contrast to the observations in the upper 50 m in Holes 971D and 971E. The overall trends of the GRAPE density are similar to those observed in the index properties density data.

Thermal Conductivity

Thermal conductivity at Hole 971A was sampled once per section in all cores from Hole 971A (Table 11, Fig. 38). Thermal conductivity values generally increase with depth from 1.0 to 1.6 W/(m · K), with large variation between 3 and 8 mbsf. The abrupt decrease of porosity at 16 mbsf (Fig. 34) does not affect the thermal conductivity.

DOWNHOLE MEASUREMENTS

Logging Operations and Quality of the Logs

A set of data from the split Quad combination (seismic-stratigraphic and litho-porosity tool strings) and Formation MicroScanner (see "Explanatory Notes" chapter, this volume) was acquired in Hole 971B. The Lamont-Doherty temperature logging tool was attached to the bottom of the litho-porosity string. After drilling and coring operations were completed in Hole 971B, the borehole was conditioned with KCl mud. The base of the BHA was set at 82.4 mbsf and pulled up to 59.5 mbsf for logging. Owing to an electronic failure, the TLT did not record during logging and no temperature data were obtained.

The lower part of the hole filled with material that collapsed from the borehole walls before and between logging operations. The bottom of the hole was encountered during the first run at 171.2 mbsf (indicating more than 30 m of fill, which is 10 m more than when cleaning operations ended) and at 136.1 mbsf during the second run (this was probably because of a bridge resulting from swelling clays). The FMS could not go farther down than 128 mbsf during the third run. Table 12 summarizes the different intervals logged with each tool string and Figure 39 shows the resulting log profiles.

The one-arm caliper measurement of the litho-porosity tool gives an indication of the borehole diameter and shows big variations from 33 cm to more than 46 cm (maximum extent of the caliper) in most of the logged interval. The fluctuations in borehole diameter can be related to lithologic or textural changes of the formation. The shape of the borehole also has some influence on the quality of the density, sonic velocity, neutron porosity, and FMS data.

The FMS images are of low quality overall owing to hole enlargement and very poor pad contact. Some evidence of the presence of clasts is locally seen, but the images are not reliable.

Results and Interpretation

Bad borehole conditions, short logged intervals, and poor core recovery all prevent detailed interpretation and good core-log integration. The sequence cored and logged is rather homogeneous (defined as a mud debris flow; see "Lithostratigraphy" section, this chapter), and thus the commonly used term "log unit" is here not appropriate. We propose subdivision of the logged section into three intervals characterized by some changes in the different physical parameters measured. Throughout the whole logged interval, the natural gamma-ray log shows intermediate values ranging from 30 to 45 GAPI, with a quite constant profile, except for the last 7 m logged, which shows increasing values to 65 GAPI. The uranium and thorium contents are characteristic of a marine clayey mud, with several spikes in both curves that may indicate shale or sand layers.

Interval 1 (60 to 100 mbsf) is characterized by a constant resistivity profile that ends at 100 mbsf with a sharp negative spike. The natural gamma-ray profile shows no significant variations, but some trends (77 to 81, 81 to 85, and 85 to 95 mbsf) in the spectral profile, also seen either in the uranium or in the thorium profile, may represent fining-upward sequences. The spectral gamma-ray as well as the thorium and uranium content profiles show relative large-scale variations at the end of Interval 1 that correlate with a negative spike in resistivity and a decrease in bulk density. This may indicate the existence of a more porous sand layer, interbedded with the mud sequence, which possibly acted as an aquifer. The caliper curve also shows a washout zone over the 95 to 100 mbsf interval, which supports this hypothesis. The pore-water chemistry results (see "Inorganic Chemistry" section, this chapter) suggest the existence of a hypersaline solution in this area, percolating through the formation. This brine could use the sand layers as conduits because of their high permeability.

Interval 2 (100 to 120 mbsf) shows a slightly increasing resistivity profile and its end is again marked by a sharp decrease in resistivity. At about 114 mbsf, we noticed the presence of a 3-m-thick zone characterized by a significant decrease in borehole diameter, an increase in natural gamma-ray, a slight increase in resistivity, and followed by a sharp negative spike in sonic velocity.

The third interval begins at 120 mbsf with the same large variations in almost all the parameters that were observed at the end of Interval 1. This layer is also characterized by bad borehole conditions,

Table 12. Hole 971B logged depth intervals for the three tool strings.

String	Run	Open-hole depth (mbsf)	Open-hole depth (mbrf)	In-pipe depth (mbsf)	In-pipe depth (mbrf)	Tools
Seismic-stratigraphic	Down	82.4–153.9	2236.4–2307.9	56–82.4	2210–2236.4	NGT/SDT/DIT
	Up 1	171.2–59.5	2325.2–2213.5	59.5–0	2213.5–2154	
	Up 2 (repeat section)	160.7–85.8	2314.7–2239.8			
Litho-porosity	Up 1	134–59.5	2288–2213.5	59.5–51.7	2213.5–2205.7	NGT/HLDT/CNT/TLT
	Up 2 (repeat section)	136.1–82.8	2290.1–2236.8			
FMS	Up 1	127.9–73.9	2281.9–2227.9			NGT/GPIT/FMS
	Up 2	128–59.5	2282–2213.5	59.5–53.7	2213.5–2207.7	

but here the variations of the density and the PEF are wider and better defined. Thorium and uranium content shows a relatively large decrease at the same depth, which is different in behavior than the bottom of Interval 1, where these values go up rather than down. This suggests that the layer between 122 and 127 mbsf has a different texture or lithology than the layer between 95 and 100 mbsf. The sequence below is characterized by an increase in resistivity from lower than 0.5 Ωm to 0.65 Ωm, by a general increase in thorium content, and by a general decrease in uranium. It corresponds to the appearance of small clasts in the cores (approximately 126 mbsf, see "Lithostratigraphy" section, this chapter). A thorium-poor zone, correlated with a negative spike in resistivity, and surrounded by two positive incursions of the thorium content at 141 and 147 mbsf can be related to a 1-m-thick clast-free zone seen in Section 160-971B-17X-1, 0–100 cm (see "Lithostratigraphy" section, this chapter).

SUMMARY AND CONCLUSIONS

The Napoli mud volcano was drilled in the Olimpi field south of Crete. Site-survey data confirm that the mud dome is an asymmetrical flat-topped structure, with a well-defined peripheral moat and underlying inward-dipping reflectors. Hole 971A (106 mbsf) was drilled just beyond the moat to investigate the margin of the mud volcano; Hole 971B (204 mbsf) was drilled within the moat; Hole 971C (17 mbsf) was drilled at the same site to recover unusual diatomaceous muds; whereas Holes 971D (46 mbsf) and 971E (29 mbsf) were both drilled to investigate the crestal area.

In Hole 971A, the sediments comprise interbedded nannofossils ooze, nannofossil clays, and turbidites ranging from middle-late Pleistocene to middle Pliocene age. This sediment is underlain by clast-rich, matrix-supported mud debris flows (16.5–71.0 mbsf). The clasts (15–25 vol%) are mainly calcareous and range from several millimeters to a few centimeters in size. The matrix of the mud debris flows contains Pleistocene, middle Miocene, Oligocene, and Eocene nannofossils. The pelagic sediment above the mud debris flow is dated as more than 0.46 Ma old, whereas that beneath the mud debris flow is younger than 1.5 Ma. In addition, the lower part of the debris flow is within the *Gephyrocapsa* Zone of 1.25–1.5 Ma age. Clasts in the mud debris flows were dated as Burdigalian to Langhian in age. In addition, the Miocene clasts contain rare nannofossils and planktonic foraminifers of Oligocene, Eocene, and Cretaceous age. The section ends with hemipelagic sediments.

Within the moat (Hole 971B) an upper unit of hemipelagic sediments with sapropels (0–20 mbsf) is underlain by mud debris flows that are older than 0.26 Ma, but younger than 0.46 Ma. Clast-poor mud debris flows alternate with more homogeneous silty clay. The matrix and the clasts in the mud debris flows are similar to those in Hole 971A; however, Pleistocene species are more abundant in Hole 971B.

Downhole logs (especially the natural gamma and resistivity) indicate the presence of a number of thin layers that correspond to relatively sandy cored intervals. Intervals with unusual compaction trends may correspond to the recovery of soupy sediment. The logs also distinguish clast-rich and clast-poor intervals.

Hole 971C, at the same location, recovered an expanded section. A 3.3-m-thick sapropel S5 is composed of laminated diatom ooze, with well-preserved diatom species characteristic of upwelling, as well as mat-forming varieties. Some radiolarians are also present.

Hole 971D, near the crest of the structure, recovered mousselike silty clay with scattered small (<5 cm) clasts of mudstone and siltstone. In addition, angular fragments of coarsely crystalline halite (up to 3 cm in size) are concentrated in thin, more silty layers, together with a small number of subrounded halite-cemented mudstone clasts (<5 cm in size). The matrix contains dominantly reworked middle Miocene nannofossils, with rare late Pleistocene age forms in the upper part of the section.

Hole 971E, also within the crestal area, comprises mousselike (i.e., gaseous) silty and sandy clays with a few small (<3 cm) clasts of mudstone and fine-grained carbonate. Rare nannofossils of late Pleistocene age are present in the upper part of the section, whereas reworked Miocene nannofossils dominate beneath this.

Gas is abundant in the Napoli mud volcano. The methane/ethane ratios in Holes 971B, 971D, and 971E vary from 10 to 40 overall, but in the individual holes values remain constant with depth. In contrast to the Milano mud volcano, no indication for the presence of methane hydrates (clathrates) was found. The gas also contains several higher hydrocarbons up to hexane and a number of hydrocarbons that could not be identified on the ship. The measured organic carbon of the organic-rich layers in the pelagic intervals is in the range typical of Pleistocene (approximately 2%–6%) and Pliocene (up to 24%) sapropels. Again in contrast to the Milano mud volcano, pore waters from the crestal holes are saturated with respect to halite in all five holes. Brines in the lower part of Hole 971A are unusually rich in potassium, suggesting that brine of more than one source may be present. The very high alkalinity throughout (approximately 80 mmol/L in Holes 971D and 971E) was probably formed by the microbial consumption of methane. The sharp downward decrease in sulfate observed in Hole 971B indicates high bacterial sulfate reduction rates and an organic-matter-rich substrate. A single ADARA temperature measurement obtained in Hole 971D at 45 mbsf gave a temperature of 16.1°C, which is 2°C above normal bottom-water levels.

The sediments cored from the Napoli mud dome all show clear evidence of sedimentary layering and an origin by the intrusion of mud sills can be excluded. The well-developed moat contains layered muddy debris flows with few clasts, compared to the thick clast-rich mud debris flows recovered at the Milano mud volcano (Hole 970A). More clast-rich mud debris flows interfinger with hemipelagic sediment on the flanks, as observed in the Milano mud volcano. The presence of more silty sediment in the crestal sites may relate to contrasting mode of eruption or the effects of current winnowing. Solid halite in the crestal holes (Hole 971D) was introduced both as crystalline aggregates and as halite-cemented clasts. Hydrocarbon gas is continuously flowing to the surface in the Napoli mud volcano and clathrates are absent (both in contrast to the Milano mud volca-

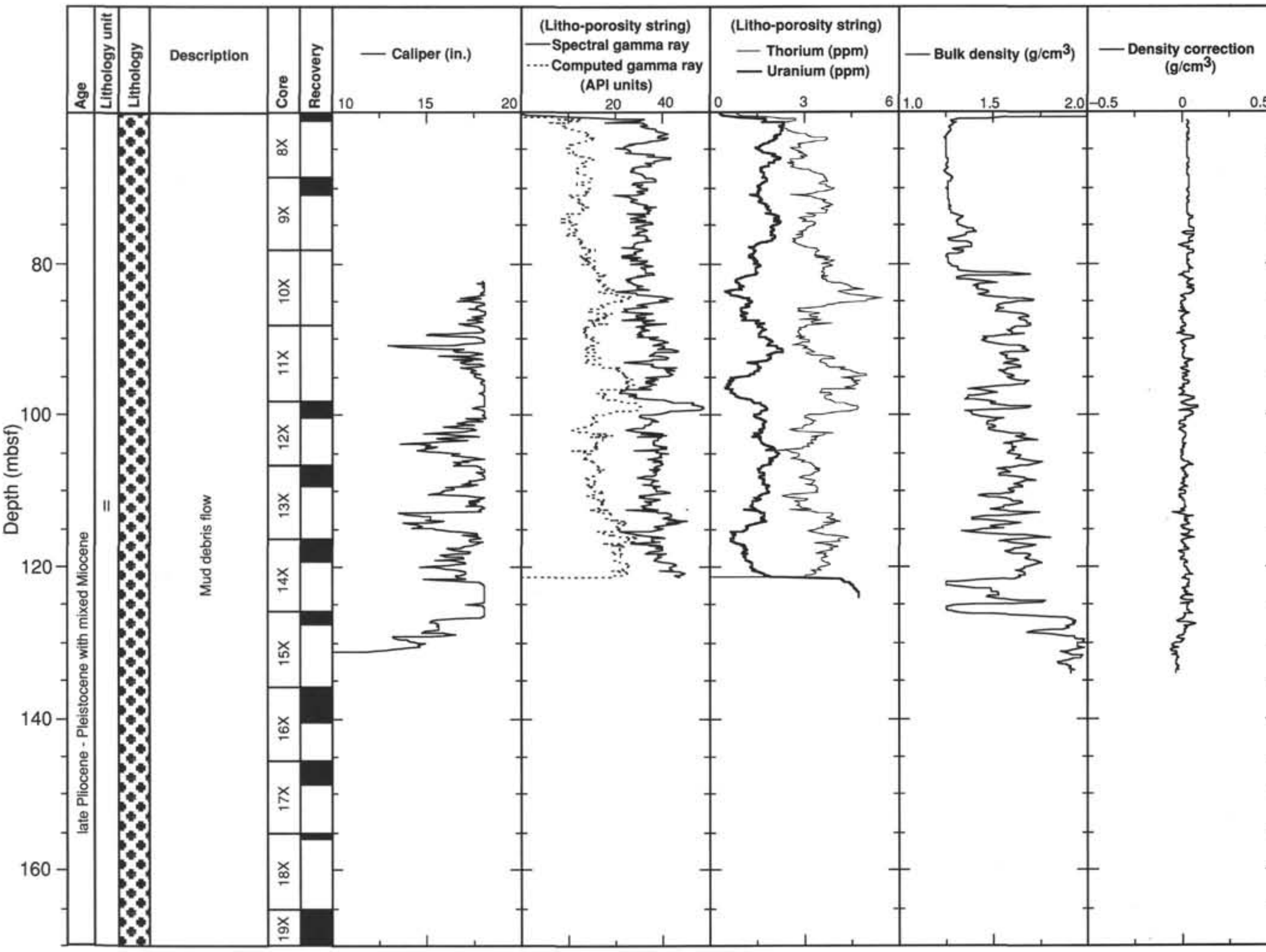

Figure 39. Hole 971B Quad combination tool results.

no), perhaps because of the effects of higher pore-fluid temperatures and salinities of up to 300 mg/kg. The Napoli mud volcano apparently first erupted between 1.5 and 1.25 Ma and was then episodically active to the present time, in contrast to the Milano mud volcano, which is probably now dormant.

REFERENCES

Brown, K., and Westbrook, G.K., 1988. Mud diapirism and subcretion in the Barbados Ridge accretionary complex: the role of fluids in accretionary processes. *Tectonics*, 7:613–640.

Brumsack, H.-J., Zuleger, E., Gohn, E., and Murray, R.W., 1992. Stable and radiogenic isotopes in pore waters from Leg 127, Japan Sea. *In* Pisciotto, K.A., Ingle, J.C., Jr., von Breymann, M.T., Barron, J., et al., *Proc. ODP, Sci. Results*, 127/128 (Pt. 1): College Station, TX (Ocean Drilling Program), 635–650.

Camerlenghi, A., Cita, M.B., Della Vedova, B., Fusi, N., Mirabile, L., and Pellis, G., 1995. Geophysical evidence of mud diapirism on the Mediterranean Ridge accretionary complex. *Mar. Geophys. Res.*, 17:115–141.

Camerlenghi, A., Cita, M.B., Hieke, W., and Ricchiuto, T.S., 1992. Geological evidence for mud diapirism on the Mediterranean Ridge accretionary complex. *Earth Planet. Sci. Lett.*, 109:493–504.

Cita, M.B., Woodside, J.M., Ivanov, M.K., Kidd, R.B., Limonov, A.F., and Scientific Staff of Cruise TTR3 Leg 2, in press. Fluid venting from a mud volcano in the Mediterranean Ridge diapiric belt. *Terra Nova*.

————, 1994. Fluid venting, mud volcanoes and mud diapirs on the Mediterranean Ridge. *Rend. Fis. Acc. Lin. Roma*, 5:161–169.

Emerson, S., and Hedges, J.I., 1988. Processes controlling the organic carbon content of open ocean sediments. *Paleoceanography*, 3:621–634.

Henry, P., LePichon, X., Lallement, S., Foucher, J.-P., Westbrook, G., and Hobart, M., 1990. Mud volcano field seaward of the Barbados accretionary complex: a deep-towed side scan sonar survey. *J. Geophys. Res.*, 95:8917–8929.

Limonov, A.F., Woodside, J.M., and Ivanov, M.K. (Eds.), 1994. *Mud Volcanism in the Mediterranean and Black Seas and Shallow Structure of the Eratosthenes Seamount.* UNESCO Rep. Mar. Sci., 64.

Manheim, F.T., and Sayles, F.L., 1974. Composition and origin of interstitial water of marine sediments based on deep sea drilled cores. *In* Goldberg, E.D. (Ed.), *The Sea* (Vol. 5): New York (Wiley Interscience), 527–568.

Rohling, E.J., 1994. Review and new aspects concerning the formation of eastern Mediterranean sapropels. *Mar. Geol.*, 122:1–28.

Schaefer, R.G., and Leythaeuser, D., 1984. C_2–C_8 hydrocarbons in sediments from Deep Sea Drilling Project Leg 75, Holes 530A, Angola Basin, and 532, Walvis Ridge. *In* Hay, W.W., Sibuet, J.-C., et al., *Init. Repts. DSDP*, 75 (Pt. 2): Washington (U.S. Govt. Printing Office), 1055–1067.

Schrader, H., and Matherne, A., 1981. Sapropel formation in the eastern Mediterranean Sea: evidence from preserved opal assemblages. *Micropaleontology*, 27:191–203.

Shipboard Scientific Party, 1984. Site 545. *In* Hinz, K., Winterer, E.L., et al., *Init. Repts. DSDP*, 79: Washington (U.S. Govt. Printing Office), 81–177.

Staffini, F., Spezzaferri, S., and Aghib, F., 1993. Mud diapirs of the Mediterranean Ridge: sedimentological and micropalaeontological study of the mud breccia. *Riv. Ital. Paleontol. Stratigr.*, 99:225–254.

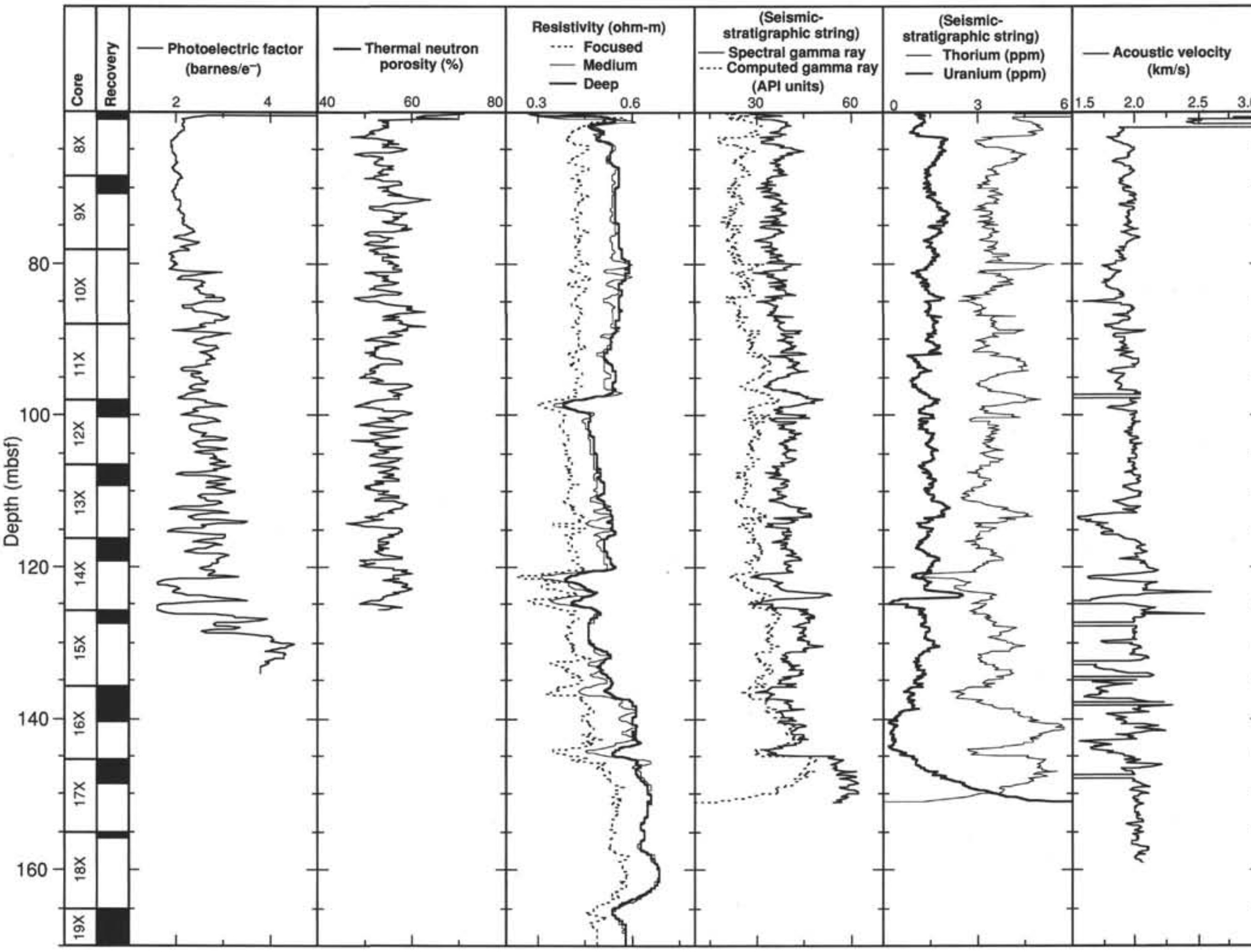

Figure 39 (continued).

Van Santvoort, P.A., and de Lange, G.J., in press. Messinian salt fluxes into the present-day Mediterranean: implication for models and budget calculations. *Mar. Geol.*

Volgin, A.V., and Woodside, J.M., in press. Sidescan sonar images of mud volcanoes from the Mediterranean Ridge: causes of variation in backscatter intensity. *Mar. Geol.*, Spec. Iss.

Westbrook, G.K., Carson, B., Musgrave, R.J., et al., 1994. *Proc. ODP, Init. Repts.*, 146 (Pt. 1): College Station, TX (Ocean Drilling Program).

Ms 160IR-112

NOTE: Core-description forms ("barrel sheets") and core photographs can be found in Section 5, beginning on page 535. Forms containing smear-slide data can be found in Section 6, beginning on page 951. Color reflectance, physical properties, chemistry, and thin-section data are presented on the CD-ROM (back pocket).

SHORE-BASED LOG PROCESSING
HOLE 971B

Bottom felt: 2152.3 mbrf
Total penetration: 203.5 mbsf
Total core recovered: 64.2 m (31%)

Logging Runs

Logging string 1: DIT/SDT-LSS/NGT
Logging string 2: HLDT/CNTG/NGT
Logging string 3: FMS/GPIT/NGT (2 passes)

The wireline heave compensator was used to counter ship heave resulting from the mild sea conditions.

Bottom Hole Assembly

The following depths for the BHA are as they appear on the logs after differential depth shift (see **Depth shift** section) and depth shift to the seafloor. As such, there might be a discrepancy with the original depths given by the drillers on board. Possible reasons for depth discrepancies are ship heave, use of the wireline heave compensator, and drill string and/or wireline stretch.

DIT/SDT-LSS/NGT: BHA at ~61 mbsf.
HLDT/CNTG/NGT: BHA at ~ 61 mbsf.
FMS/GPIT/NGT: did not reach BHA (pass 1).
FMS/GPIT/NGT: BHA at ~ 63 mbsf (pass 2).

Processing

Depth shift: All original logs were interactively depth shifted with reference to the NGT from the DIT/SDT-LSS/NGT run and to the seafloor (2152.3 mbrf).

Gamma-ray processing: The NGT data were processed to correct for borehole size and type of drilling fluid.

Acoustic data processing: The sonic logs were processed to eliminate some of the noise and cycle skipping experienced during recording.

Quality Control

Data recorded through the BHA, such as the NGT and CNT data above 61 mbsf, should be used only qualitatively because of the attenuation on the incoming signal. Invalid NGT data were recorded at 35–38.5 mbsf.

Hole diameter was recorded by the hydraulic caliper on the HLDT tool (CALI) and the caliper on the FMS string (C1 and C2).

Details of standard shore-based processing procedures are found in the "Explanatory Notes" chapter (this volume). For further information about the logs, please contact:

Cristina Broglia
Phone: 914-365-8343
Fax: 914-365-3182
E-mail: chris@ldeo.columbia.edu

Elizabeth Pratson
Phone: 914-365-8313
Fax: 914-365-3182
E-mail: beth@ldeo.columbia.edu

Hole 971B: Natural Gamma Ray-Density-Porosity Logging Data

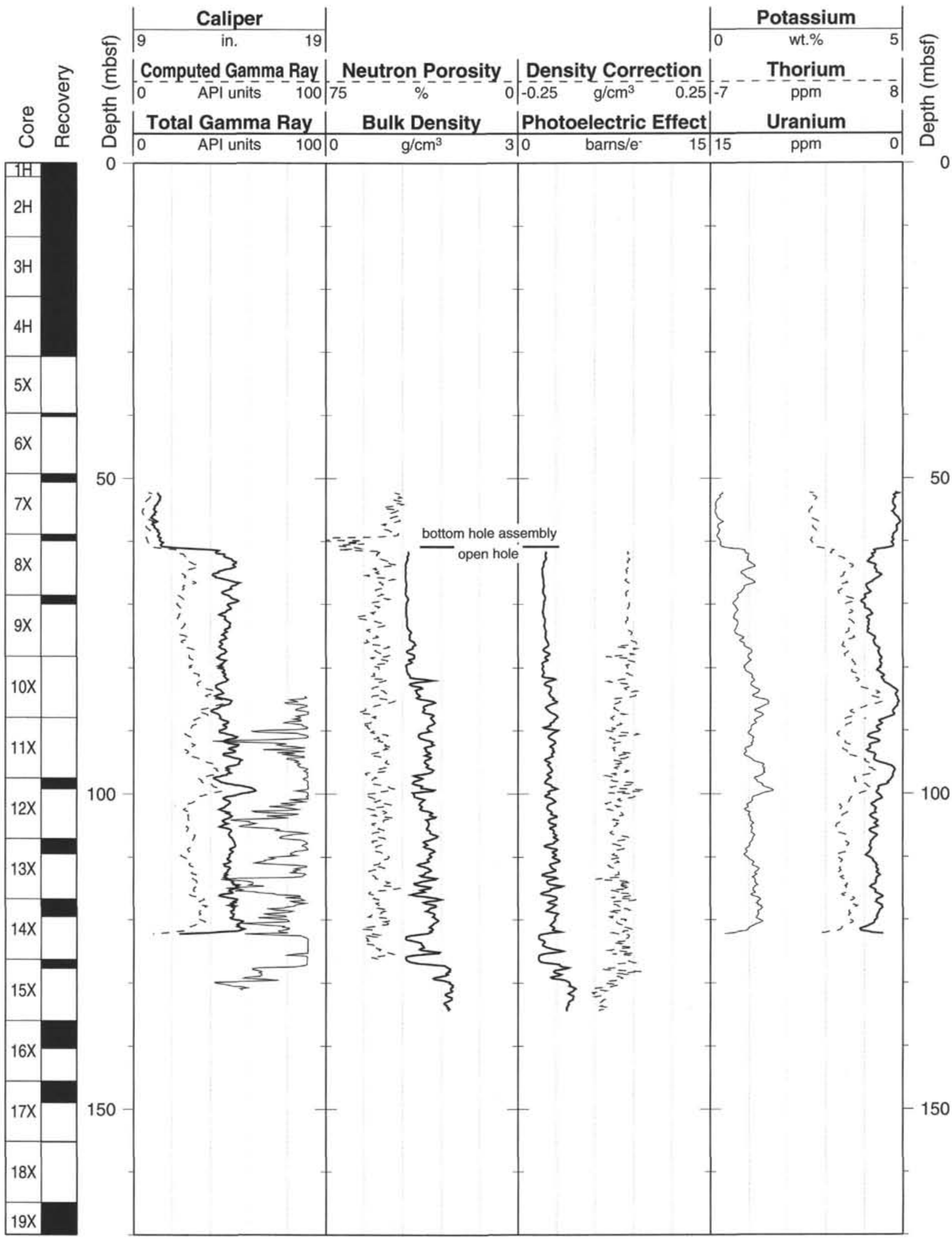

Hole 971B: Natural Gamma Ray-Resistivity-Sonic Logging Data